DEVELOPMENT OF RADAR ALTIMETRY DATA PROCESSING IN THE OCEANIC COASTAL ZONE

ESA/ESRIN Contract No. 21201/08/I-LG (CCN 2)

Deliverable on

Wet Tropospheric Corrections in Coastal Areas

Version 1.2

Code	COASTALT-D21b-12	**Edition**	1.2	**Date**	30-06-09
Client	European Space Agency	**Final User**		-	

	Name	Signature	Date
Written by	UPorto (Joana Fernandes, Clara Lázaro and Alexandra Nunes)		24/04/2009
Approved by			
Revised by			
Authorised by			

DISSEMINATION	COPIES	MEANS
ESA, Jérôme Benveniste and Salvatore Dinardo	1	Electronic
NOCS, Paolo Cipollini	1	Electronic

SUMMARY OF MODIFICATIONS

Ed.	Date	Chapter	Modification	Author/s
1.2	30/06/2009		ACRONYMS section added	UPorto
			Equation (1) corrected	UPorto

TABLE OF CONTENTS

Acronyms

2T - 2-meter Temperature
AMR - Advanced Microwave Radiometer
AVISO - Archiving, Validation and Interpretation of Satellite Oceanographic data
BKG - Bundesamt für Kartographie und Geodäsie
CDDIS - Crustal Dynamics Data Information System
CORSSH - Corrected Sea Surface Height
DLM - Dynamically-Linked Model
ECMWF - European Centre for Medium-range Weather Forecasts
EPN - EUREF Permanent Network
ERS - European Remote Sensing Satellite
ESA – European Space Agency
F-PAC – French Processing and Archiving Facility
GDR - Geophysical Data Record
GFO - Geosat Follow-On
GMF - Global Mapping Functions
GNSS - Global Navigation Satellite System
GPD - GNSS-derived Path Delay
GPS - Global Positioning System
IGS - International GNSS Service
IWV - Integrated Water Vapour
JMR - Jason-1 Microwave Radiometer
MIT – Massachusetts Institute of Technology
MWR - MicroWave Radiometer
NCEP - National Center for Environmental Prediction (USA)
NWM – Numerical Weather Model
OA - Objective Analysis
PISTACH – Prototype Innovant de Système de Traitement pour l'Altimétrie Côtière et l'Hydrologie
PW - Precipitable Water
RADS - Radar Altimeter Database System
RINEX - Receiver INdependent EXchange format
RMS – Root Mean Square
STD - Slant Total Delay
T/P - TOPEX/Poseidon
TB – Brightness Temperature
TB23 – Brightness Temperature at the 23 GHz channel
TCWV - Total Column Water Vapour
TMR - T/P Microwave Radiometer

UPorto - University of Porto
UTC – Coordinated Universal Time
VMF1 - Vienna Mapping Functions 1
WMO - World Meteorological Organization
ZHD - Zenith Hydrostatic Delay
ZTD - Zenith Total Delay
ZWD – Zenith Wet Delay

Introduction

This document presents the Deliverable D2.1b for the COASTALT project, CCN 2, SUB-CONTRACT COASTALT TO ESRIN CONTRACT N. 20698/07/I-LG. This document is delivered for fulfillment of milestone M2b.

The present report describes the work that has been done at University of Porto (UPorto) in the development of the two proposed algorithms for deriving the wet tropospheric correction for coastal altimetry: the Dynamically-Linked Model (DLM) and the GNSS-derived Path Delay (GPD) approaches. The document is divided in four sections. Section 1 introduces and briefly describes the data sets used throughout the document. Sections 2 and 3 present the DLM and GPD approaches, respectively. The main conclusions are summarized in section 4.

1 Datasets

1.1 Introduction

This study has been conducted using various data types that will be briefly described in this section. These include tropospheric delays present in the altimeter datasets, GNSS (Global Navigation Satellite System) derived tropospheric delays from UPorto (University of Porto, Portugal) and EUREF solutions), and data from ECMWF (European Centre for Medium-range Weather Forecasts).

In this study two periods of analysis have been selected:

Period A, September 2002 to August 2005 - a 3-year period which has been selected as the unique period for which there were four altimeter missions with different ground tracks: TOPEX/Poseidon (T/P), Jason-1, Envisat and Geosat Follow-On (GFO) (Figure 1).

Period B, January 2002 to December 2007 – a 6-year period which has been selected as the largest period for which there are continuous data from Envisat and Jason-1, and GNSS data from UPorto solutions for a selected network of 13 stations (represented in Figure 1).

Apart from some global analyses which are reported throughout the document, in most parts of the study data have been analysed for the European region presented on Figure 1 ($30^\circ \leq \varphi \leq 55^\circ$, $-20^\circ \leq \lambda \leq 5^\circ$). Inside this region two subregions have been selected: the NW Iberian region (a validation zone for COASTALT) and the West Mediterranean region (coincident with the ESA-funded project PISTACH test region).

1.2 Description of datasets

1.2.1 Altimetry

For the purpose of comparing the tropospheric corrections present on the altimeter GDR (Geophysical Data Record) fields (dry and wet corrections) with the corresponding fields derived by GNSS (Zenith Hydrostatic and Wet Delays: ZHD and ZWD), altimeter data have been selected from two well known databases: RADS (Radar Altimeter Database System) and AVISO (Archiving, Validation and Interpretation of Satellite Oceanographic) data.

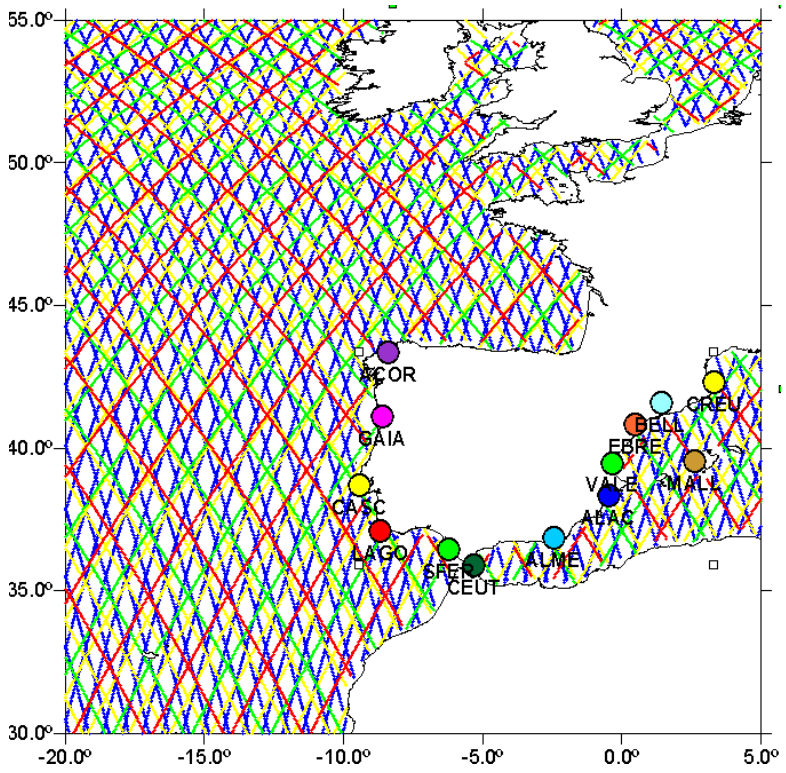

Fig.1 – Study area: altimeter ground tracks of Topex/Poseidon (red), Jason-1 (green), Envisat (blue), GFO (yellow) and location of the regional network of 13 stations used in the data comparison study.

AVISO data are the Corrected Sea Surface Height (CORSSHs, (AVISO 2005)) as downloaded in the beginning of 2008. RADS data are the data available as on 29 March 2009. Since RADS does not provide, at present, an informative document, the information presented here is from Remko Scharroo personal communication.

From the initial work performed with AVISO data, it became clear that not enough information was available on data processing and editing. In addition, the data included track points very close to the coast which, in the absence of flags signaling the land influence, could not be properly edited.

For this reason, it was decided to use the RADS data in most part of the study and only this dataset will be described here.

As referred above, data from four missions have been selected: T/P, Jason-1, Envisat and GFO.

Concerning the tropospheric fields present on RADS, the dry correction (Zenith Hydrostatic Delay, ZHD) is from ECMWF for Envisat, Jason-1 and T/P and from NCEP (National Center for Environmental Prediction, USA) for GFO. The wet correction (Zenith Wet Delay, ZWD) is the microwave radiometer (MWR) based correction from the various missions.

Concerning the MWR-based corrections, the following updates are performed in RADS:

Envisat: At the beginning of Cycle 51, the Envisat MWR processing at F-PAC includes a side-lobe correction. This is intended to better model land contamination in the side lobes. The product containing the corrected TBs has

been provided to RADS by ESA and has been incorporated, for cycles up to 50. For cycles 51 onwards this effect is already included in the Envisat GDRs. So, in RADS this effect is applied to all cycles in a consistent way.

In RADS a drift to the TB23 is also applied: $TB23' = TB23 + 0.156 \cdot t \ (K)$, where t is time in years since 19-Oct-2002. The wet tropospheric correction is then recomputed using the corrected TB (TB23').

Jason-1: The GDR-B data had wet tropospheric corrections that were too wet by approximately 2.3%. Originally the data were corrected by scaling the wet tropospheric correction by 0.9775. In October 2008, Shannon Brown provided correction products, with recalibrated JMR (Jason-1 Microwave Radiometer) data, the same as those present in GDR-C. Present RADS data incorporates these JMR corrections, that is, they correspond to Jason-1 GDR-C products.

In addition, according to Shannon Brown personal communication, the JMR data on the GDR are all shifted down the track by one second. This error is made during the interpolation of the JMR data along the altimeter ground track. RADS compensates for this by moving all radiometer data (wet tropospheric correction, brightness temperatures and water vapour estimates) one second backwards. The sigma0 attenuation correction is not adjusted. This problem is also affecting Jason-2 AMR (Advanced Microwave Radiometer) data present on GDRs.

T/P: In March 2007, Shannon Brown provided a TMR (T/P Microwave Radiometer) correction product. TMR had a drift, and besides, the algorithm provided a wet tropospheric correction about 2.3% too wet. Present RADS data incorporates the TMR corrections from the TMR correction product.

GFO: In RADS the GFO brightness temperatures are not changed with respect to GDRs, but a different model is used for the wet tropospheric correction than is on the GFO GDRs.

Previous to any analysis, altimeter data have been stacked, i.e. interpolated into reference points along altimeter reference tracks.

In addition to the above mentioned data sets (RADS and AVISO) data from Envisat GDRs have been used in various parts of the study.

1.2.2 GNSS tropospheric data

Two types of GNSS data are available for both the two periods referred above and for the same network of 13 stations in the West European region illustrated on Figure 1: ZHDs + ZWDs from UPorto solutions corrected for station height, i.e. data has been reduced to sea level; ZTDs (Zenith Total Delays) computed at EUREF centres available online at the same stations not corrected for station height, i.e. data refer to station height.

1.2.2.1 UPorto

UPorto solutions have been computed at 1-hour interval using VMF1 (Vienna Mapping Functions 1) – see details below. From in situ pressure data at each station (where available) or from the VMF1 grids, using the

Saastamoinen (1972) model, the ZHD has been computed. Finally, by subtracting the ZHD from the ZTD, the ZWD has been obtained.

For comparison with altimeter corrections, UPorto ZHD and ZWD solutions have been separately reduced to sea level according to the procedure described later.

1.2.2.2 EUREF

EUREF solutions have been computed using GMF (Global Mapping Functions) - or even coarser - mapping functions and are provided at 1 hour interval.

Note that EUREF solutions do not contain enough information to allow the separation of ZTD into a sum of ZHD and ZWD and therefore, for the computation of height reduction. For that purpose pressure data from in situ measurements or from a meteorological model such as ECMWF would have to be used. Later, in section 3.2.2, results will be presented for the estimation of ZHD from global VMF1 grids for the EUREF stations.

1.2.3 ECMWF atmospheric fields

ECMWF (European Centre for Medium-range Weather Forecasts) provides global 0.25°×0.25° grids of several weather-related parameters every 6 hours (00 UTC, 06 UTC, 12 UTC and 18 UTC) (ECMWF 2009). In the scope of this study, the atmospheric fields of two single-level parameters of the Deterministic Atmospheric Model were obtained: surface temperature (2-meter temperature, 2T) and integrated water vapour (total column water vapour, TCWV) for a 1-year period (01/01 to 31/12, 2007) and a geographical area ranging from -20° to 20° in longitude and 30° to 60° in latitude.

2 Dynamically-Linked Model

2.1 Introduction

This section describes the Dynamically-Linked Model (DLM) approach for deriving the wet tropospheric correction for coastal altimetry.

The basic idea is to derive a simple and easy to implement procedure that requires only data from the altimeter Geophysical Data Records (GDR) and that takes full advantage of the two types of wet tropospheric corrections that are present on the GDR: the microwave radiometer (MWR) derived correction and a large-scale atmospheric reanalysis model-derived correction such as that from the European Centre for Medium-range Weather Forecast (ECMWF).

The method consists in replacing, in the coastal regions, the invalid MWR-derived correction by the model correction, somehow dynamically linked to the closest points with valid MWR field, to warrant continuity.

It should be emphasized that this approach is significantly different from the use of the ECMWF model correction everywhere. It is well known that the wet tropospheric models are not suitable for processing long time series of satellite

altimetry since they possess long-term errors and discontinuities (e.g. Scharroo et al. 2004). In addition, they possess small-scale errors, which may be due to mislocation and absence of some atmospheric features. Although this method does not compensate for the small-scale errors, it significantly reduces the large-scale ones. This happens because the large-scale errors for small regions, such as land contaminated tracks in coastal zones, are quasi-linear and will be removed by locally adjusting the model to the radiometer field.

The method requires information available on the GDR with optional information from a distance-to-land global grid and can be implemented globally for any satellite. The question is then on which particular strategy should be adopted to ensure the continuity in the transition between radiometer and model fields.

2.2 Method

At the very beginning, the algorithm needs to identify the “microwave radiometer land-contaminated zones”, that is, the coastal track segments that contain groups of points with invalid MWR field, which therefore need to be corrected. The definition of these land-contaminated zones can be based on the MWR land flag, provided this is reliable.

Comparisons with GNSS-derived tropospheric delays show that in some close-to-land regions, at distances less than 30 km from the coastline, the radiometer correction can be quite noisy, while the corresponding MWR land flag is still off. These results show that the various missions use different criteria for setting the radiometer land flag. While for example T/P and Jason-1 radiometer land flag is set for all points at distances to land up to ~50 km (see Fig. 2), ERS (European Remote Sensing) for points up to ~30 km, the corresponding Envisat flag is set only in a small portion of these points and the same flag for GFO is not reliable. A detailed analysis of Envisat data shows that, for this mission, there is another set of points which are contaminated by land and that are not detected by the radiometer land flag. These points are attributed a measurement quality flag (MWR_QUAL) equal to 2, meaning that these values have been extrapolated using the last valid radiometer measurement (ESA 2006). This extrapolation has a smoothing effect on the wet correction field, so data “looks” ok. Indeed, if the actual retrieved TBs were used to compute the wet delay at these points, these would be quite noisy. The spatial distribution of these two types of Envisat flags is illustrated in Figure 2.

In conclusion, while for ERS, T/P and Jason-1 the land contaminated zones can be defined as the points with radiometer land flag equal to 1, for Envisat these points should be defined as the measurements which possess the radiometer land flag equal to 1 or the MWR_QUAL flag equal to 2. For GFO, the identification of the land contaminated zones has to be based on the points distance to land.

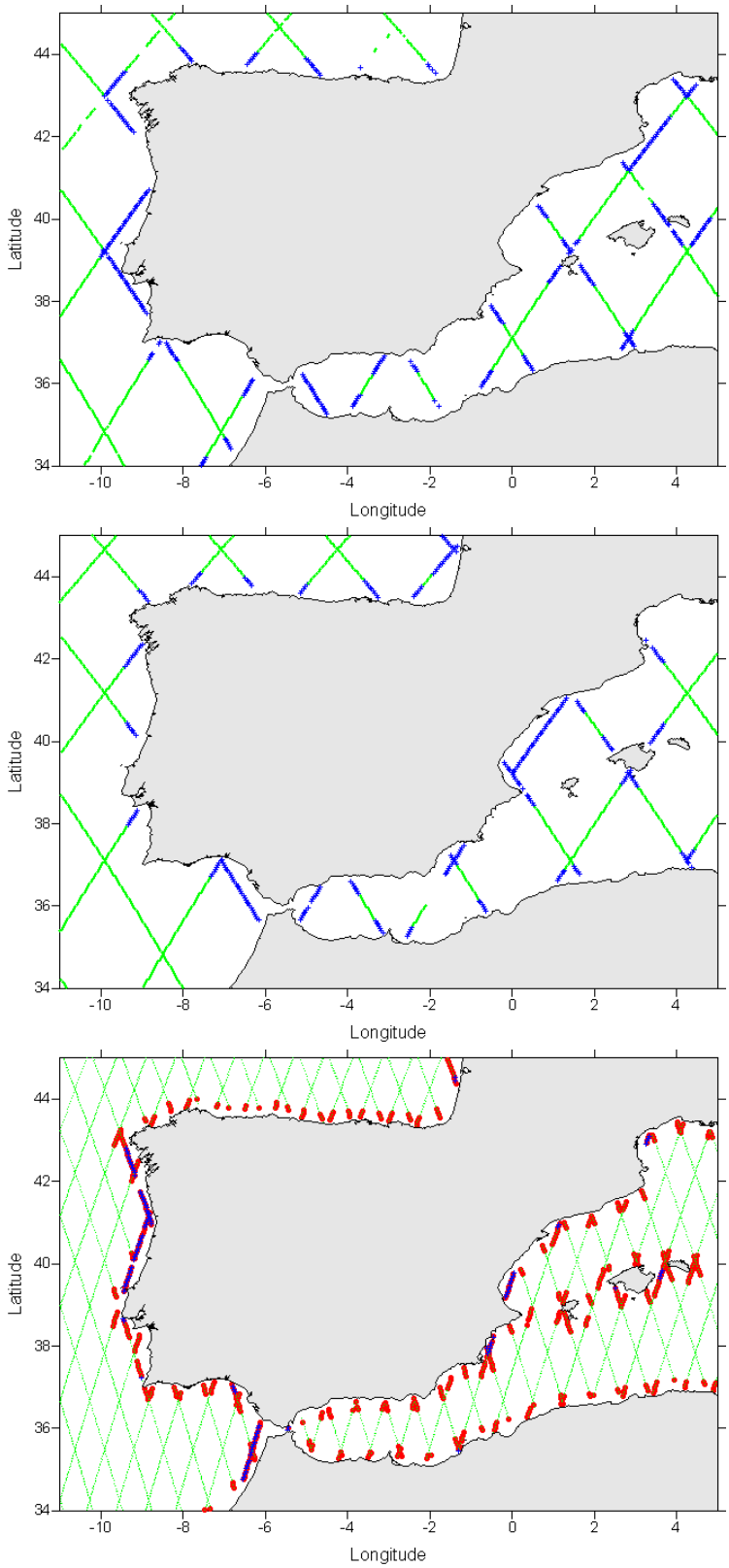

Fig.2 – Altimeter ground tracks of Jason-1 cycle 187 (top), T/P phase B cycle 422 (middle) and Envisat cycle 54 (bottom). In blue: points with radiometer land flag equal to 1. In red: points with Envisat MWR_QUAL flag equal to 2.

An alternative method to define the land contaminated zones is by using distance-to-land information and ensuring that all points with a distance-to-land smaller than a specified value, e.g. 20 or 30 km, are also considered contaminated points and must be corrected. The flags-based approach has the advantage that it only requires information present on the GDR (radiometer and model corrections and the land radiometer-related flags). The second approach depends on the quality of the coastline used to compute the distance-to-land grid and reduces the possibility that land contaminated points are left uncorrected, but might lead to the unnecessary correction of valid radiometer points. In the absence of reliable flag information for missions such as GFO, this might be the only possible approach.

Considering a simple but efficient implementation, two types of algorithms can be adopted: an island type and a continental coastline type. The first case is suggested by the land contaminated segments formed around relatively small islands or peninsulas, where a land contaminated segment is formed and there are valid radiometer points on each side of the segment. The second case happens around the continental coastlines, typically when a satellite is approaching or receding from a large land mass. In this case, there is only valid radiometer correction on one of the sides of the contaminated segment.

In the island type of algorithm, the model field is adjusted to the microwave radiometer field at the beginning and end of the land contaminated segment by using a linear adjustment. The numerical weather model correction (ZWD_{NWM}) is then dynamically linked to the microwave radiometer field (ZWD_{MWR}) at the beginning and end of the segment, for example at the first (A) and last (B) points with valid MWR correction. For all contaminated points X between A and B, the final field ($ZWD_{DLM}(X)$) will be equal to the model field plus a linear correction, ensuring that at both A and B the MWR and adjusted model fields are the same, achieving the required continuity.

$$ZWD_{DLM}(X) = ZWD_{NWM}(X) + \text{bias}(A) + \alpha \cdot (X - A) \qquad (1)$$

$$\alpha = \big(\text{bias}(B) - \text{bias}(A)\big) / \big(B - A\big)$$
$$\text{bias}(A) = ZWD_{MWR}(A) - ZWD_{NWM}(A)$$
$$\text{bias}(B) = ZWD_{MWR}(B) - ZWD_{NWM}(B)$$

In the continental coastline type of algorithm there is only valid information on one side of the contaminated segment and therefore it is not possible to perform an adjustment of the model and radiometer fields by using a linear adjustment. In this case, the adjustment is performed only at the beginning or end of the segment by using the bias correction defined in equations (1) at the first (A) or last (B) point with valid radiometer field. For all contaminated points X between the beginning of the segment and A (or between B and the end of the segment), the final field $ZWD_{DLM}(X)$ will be equal to the model field $ZWD_{NWM}(X)$ plus a bias correction, bias(A) (or bias(B)), ensuring that at A or B both fields will be the same and therefore continuous.

$$ZWD_{DLM}(X) = ZWD_{NWM}(X) + \text{bias}(A \text{ or } B) \qquad (2)$$

Prior to this implementation, altimeter data shall be separated into segments where a new segment is considered whenever a data gap greater than a specified value, e.g. 20 seconds, exists. Next, the algorithm identifies “land zones”, that is, sets of points with invalid radiometer field, using an approach as described above. The algorithm shall then be applied to each data point inside the “land zone”. In this way, the only points that will not be recovered are segments for which there are no valid radiometer points close enough to perform the adjustment (see Fig.5).

In addition to the main issues discussed above, there are other details that are important for an efficient implementation. An adequate data editing has to be performed to insure that no invalid radiometer measurements are kept outside the defined “land zones”, to avoid that the adjustment is performed to invalid data. Additional rejection criteria shall then be set, e.g. measurements contaminated by rain or ice, field value outside the interval [-0.5;0[metres, etc. Further refinements might include a redefinition of the land zones, by for example, joining zones that are only a few (1 to 3) points apart.

2.3 Results

Studies previously conducted by Fernandes et al. (2003) on ERS data, show that this simple approach leads to a data recovery of 80 to 90% of the invalid measurements in the coastal regions, does not introduce discontinuities in the correction and can be used to generate coastal products in an operational processing scheme. Mercier (2004) has also applied a similar type of algorithm to improve data recovery near the coast.

Present implementation of the algorithm has been tuned to Envisat data and uses a definition of the land zones solely based on the radiometer flags, as described above.

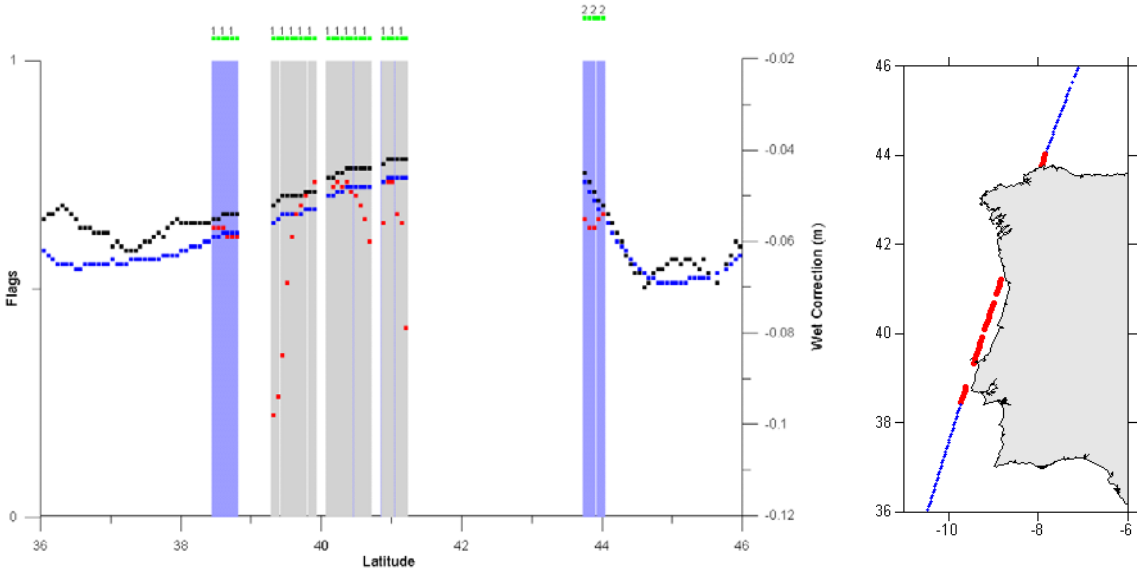

Fig.3 - Example of the implementation of the DLM algorithm for Envisat pass 160 (Cycle 54) crossing the Iberian Peninsula; The right plot illustrates the location of the pass.

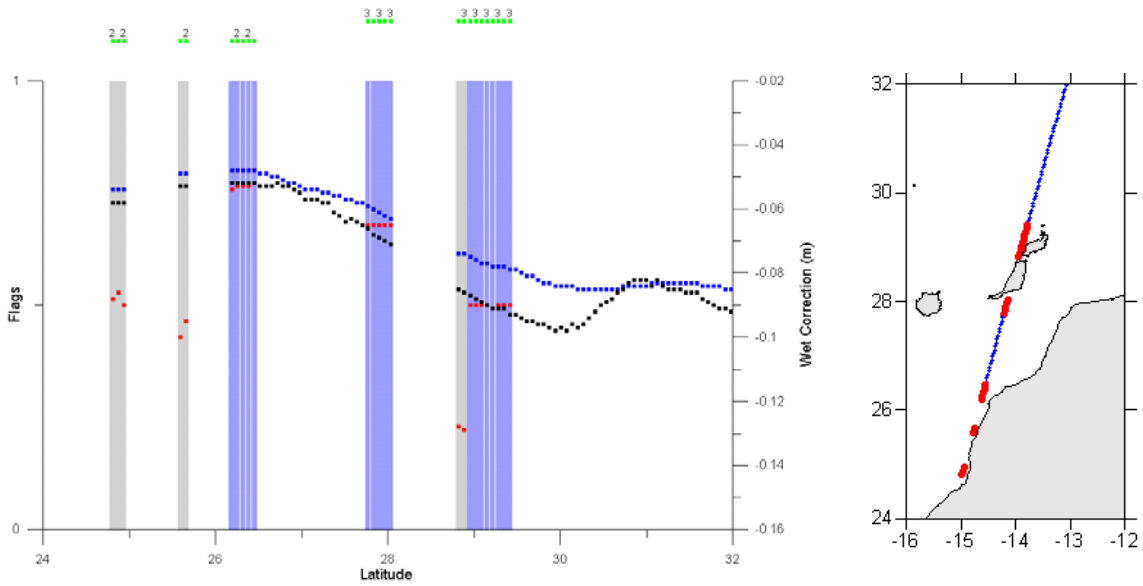

Fig.4 - Example of the implementation of the DLM algorithm for Envisat pass 246 (Cycle 54) crossing the Canary Islands and African coastline; The right plot illustrates the location of the pass.

Figures 3 and 4 illustrate two examples of the application of this algorithm to two regions: a continental coastline and a mixed region. In the maps on the right hand side of the figures, the red points represent land contaminated points in the radiometer wet tropospheric correction that must be adjusted by the algorithm.

In the graphs on the left, the blue points represent the ECMWF model correction, the red points the original microwave radiometer correction and the black points the final correction after applying the DLM algorithm. The shaded areas represent the flags that are used to identify the land contaminated points: the radiometer land flag (grey areas) and the MWR_QUAL flag (blue areas). The points for which the radiometer land flag is 1 (grey areas) usually present a radiometer correction very noisy. On the contrary, points which have MWR_QUAL flag equal to 2 (blue areas) have a nearly constant value for the radiometer correction. In any case, both types of measurements shall be corrected by the algorithm.

In the shaded land contaminated regions, the original noisy radiometer correction (in red) is replaced by the smoother correction (in black). The green dots on the top of the graphs represent the algorithm zone flag with labels associated to the type of algorithm: 1 for a continental coastline, beginning of a segment, 2 for a continental coastline, end of a segment; 3 for an island type of segment.

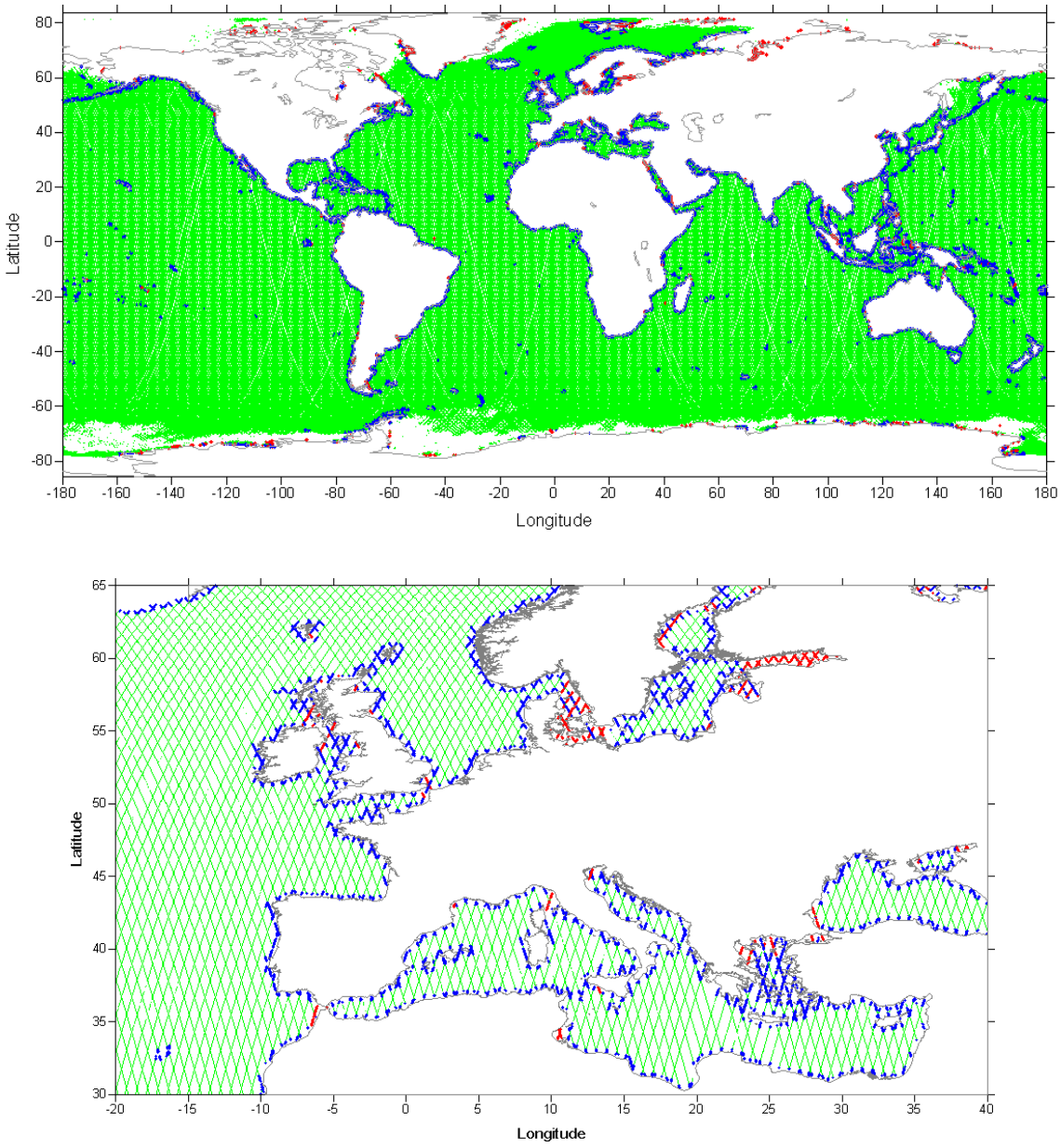

Fig.5 - DLM output for Envisat cycle 54: global result (top) and for the European region (bottom). In green: points which are not contaminated by land. In blue: points which are contaminated by land and have been adjusted by the DLM algorithm. In red: points which are contaminated by land and have not been adjusted.

Figure 5 shows the result of applying the algorithm to the whole world (top figure) and to the European region (bottom figure). for Envisat cycle 54. The blue points represent measurements that were contaminated by land and were corrected by the DLM algorithm (34488 points) while the red points represent measurements that were contaminated but were not corrected. (3302 points). On average, for Envisat, 92% of the points are adjusted. For the unadjusted measurements the output field shall be the model field corrected for the mean bias between the radiometer and the model fields, which for ECMWF is approximately 0 mm and for NCEP is 8 mm (see results below).

The accuracy of the method is directly related to the corresponding accuracy of the adopted NWM. Usually, the GDRs provide the wet tropospheric correction from two models: ECMWF and NCEP.

To inspect the differences between the wet tropospheric correction from the onboard radiometer and from the ECMWF and NCEP models, these have been compared for Envisat cycles 54 to 65, roughly corresponding to the period of the year 2007. Considering only points with valid radiometer measurement, covering the whole world (a total of 15842434 points, approximately 1440221 points per cycle), the difference between the radiometer and ECMWF corrections is 1 ± 19 mm, while the corresponding difference between the radiometer and NCEP is 8 ± 34 mm. The corresponding difference between the ECMWF and the NCEP wet tropospheric corrections is -6 ± 29 mm.

To evaluate the sensitivity of the DLM output to the adopted NWM, the algorithm has been applied to the above mentioned 11 Envisat cycles, to the whole range of latitudes and longitudes, using each of the above mentioned NWM. A total number of 430128 coastal “land contaminated points” have been corrected. For these points, the difference, which before adjustment was -7 ± 27 mm (difference between ECMWF and NCEP), reduces to -1 ± 8 mm after the DLM adjustment to the radiometer field.

Being impossible to perform an accuracy assessment of the method using radiometer measurements, this analysis gives an indication of the variability of the results, considering the accuracy of present numerical weather models. This shows that ECMWF is more precise than NCEP and that the DLM adjustment to ECMWF shall provide wet tropospheric corrections in the coastal region within an accuracy better than 1 cm.

3 GNSS-derived Path Delay

3.1 Introduction

Over the recent years an increasing number of inland GNSS (Global Navigation Satellite System) stations became available. In the scope of GPS (Global Positioning System) positioning, the tropospheric delay is often seen more as a nuisance factor, thus requiring effective estimation. Consequently, a vast number of developments have been pursued, aiming at the modelling of this effect (e.g. Saastamoinen 1972, Hopfield 1971, Niell 1996). GNSS data can be used to determine zenith tropospheric delays at the station location with an accuracy of a few millimetres (e.g. Niell et al. 2001, Snajdrova et al. 2006). The potential for the remote determination of atmospheric integrated water vapour and precipitable water also led to the development of several models mainly for meteorological purposes (e.g. Bevis et al. 1992). In the ambit of altimetry range correction, such data have been used with the purpose of calibrating the wet tropospheric correction derived from the on-board microwave radiometers (MWR) over offshore oil platforms (e.g. Bar-Sever et al. 1998, Edwards et al. 2004).

This section describes a method for obtaining the wet tropospheric correction for coastal altimetry from GNSS-derived tropospheric delays, the so called GPD (GNSS-derived Path Delay) approach. The method is based on tropospheric path delays (Zenith Hydrostatic Delays, ZHD, and Zenith Wet Delays, ZWD) precisely determined at a network of land-based or offshore GNSS stations, further combined with additional MWR measurements and output data from Numerical Weather Models (NWM), such as those produced by ECMWF.

3.2 Determination of Tropospheric Path Delays at GNSS stations

The tropospheric path delay directly derived from GNSS data is that associated to the slant path of the radio signal between a GNSS station and a satellite, caused by the hydrostatic (‘dry’) and non-hydrostatic (‘wet’) components of the neutral troposphere (e.g. Bevis et al 1992). Methodologies for estimating the wet tropospheric delay from GNSS data are, at present, well established and have been used by a vast number of authors; details can be found in Haines and Bar-Sever (1998), Desai and Haines (2004), Edwards et al. (2004) and Moore et al. (2005). A number of suitable software packages have been developed for the processing of GNSS networks with the purpose of determining the tropospheric parameters, such as GAMIT (Herring et al. 2006), GIPSY/OASIS (Webb and Zumberge 1995) and Bernese (Dach et al. 2007).

3.2.1 Software and processing strategies

3.2.1.1 GAMIT

Within this project, reference is given to the freeware GAMIT - a comprehensive GPS analysis package developed by MIT, Scripps Institution of Oceanography and Harvard University with support from the National Science Foundation - which is able to estimate a zenith path delay and its atmospheric gradient for each station, modelled in both cases by a piecewise-linear function over the span of the observations (Herring et al. 2006).

The tropospheric propagation delay is determined by GAMIT according to the following equation:

$$\mathrm{STD}(E) = \mathrm{ZHD} \times \mathrm{mf_h}(E) + \mathrm{ZWD} \times \mathrm{mf_w}(E) \qquad (3)$$

where STD is the slant total delay measured by GNSS, E is the elevation angle of the GNSS satellite and mf_h and mf_w are the mapping functions for hydrostatic and wet components, respectively (Herring et al. 2006).

A priori ZHD is evaluated from meteorological data using the modified Saastamoinen zenith hydrostatic delay model (Saastamoinen 1972, Davis et al. 1985) – equation (5) below. In this way, for each slant total delay (STD) observation a combined Zenith Total Delay (ZTD) is determined. The separation of this quantity into a sum of ZHD and ZWD depends on the accuracy of the surface pressure data (surface pressure or model) used to compute the ZHD component. At a given step interval (e.g. one hour) and for each station of the defined network, a combined ZTD is estimated from the observations to all visible satellites. For the determination of tropospheric parameters a wide span of satellite elevation angles is advisable (Niell et al. 2001). For this reason, a relatively low (e.g. 7°) elevation cut-off angle can be adopted.

3.2.1.2 Mapping Functions

In the estimation procedure, mapping functions play a major role since they are responsible for the conversion between zenith and slant delays. The most commonly used mapping functions are all based on the same equation first proposed by Marini et al. (1972): a continued fractions form in terms of sinE with coefficients a, b and c.

$$\mathrm{mf}(E,a,b,c) = \frac{1 + \dfrac{a}{1 + \dfrac{b}{1+c}}}{\sin E + \dfrac{a}{\sin E + \dfrac{b}{\sin E + c}}} \qquad (4)$$

The main differences between the several mapping functions that have been used over the last decade are the values of the adopted coefficients, their derivation, and the knowledge of atmospheric composition and structure they express. Radiosonde data (Niell 1996), ray-tracing through NWM (Niell 2001, Boehm and Schuh 2004) or climatologies (e.g. Boehm et al. 2006) have been used to derive the referred sets of coefficients.

The Vienna Mapping Functions 1 (VMF1, Boehm and Schuh 2004) are based on direct ray-tracing through NWM. The VMF1 a_W and a_H coefficients are derived from the pressure level data calculated by ECMWF and are given on a global 2.0°×2.5° latitude-longitude grid, four times a day, at 0, 6, 12 and 18h UTC (the b and c coefficients are then modelled from the respective a coefficient). VMF1 are at present the mapping functions that allow a description of the atmosphere with the finest detail, leading to the highest precision in the derived tropospheric parameters. The climatology-based Global Mapping Functions (GMF, Boehm et al. 2006) are used in GAMIT whenever VMF1 are not available.

3.2.1.3 Network design

Since all stations belonging to the same regional network, which is the case of the chosen EUREF Permanent Network (EPN) stations, shall observe a given GNSS satellite with similar viewing angles, the estimated zenith delays result highly correlated. This problem is overcome here by including in the network a set of IGS (International GNSS Service) stations located away from the study area, in the Southern Hemisphere and far Northern Hemisphere.

A collection of 57 stations from (IGS) and (EPN) was used. Daily RINEX (Receiver Independent Exchange format) files with a 30-second sampling interval provided from CDDIS (Crustal Dynamics Data Information System) and BKG (Bundesamt für Kartographie und Geodäsie) were used for the period between January 2002 and December 2007. From the selected GNSS stations, 26 belong to EPN and are located on the Iberian and North-West Mediterranean coasts. The remaining stations belong to IGS and are globally distributed, in order to provide stability to the resulting network. Figure 6 shows the location of the sites considered.

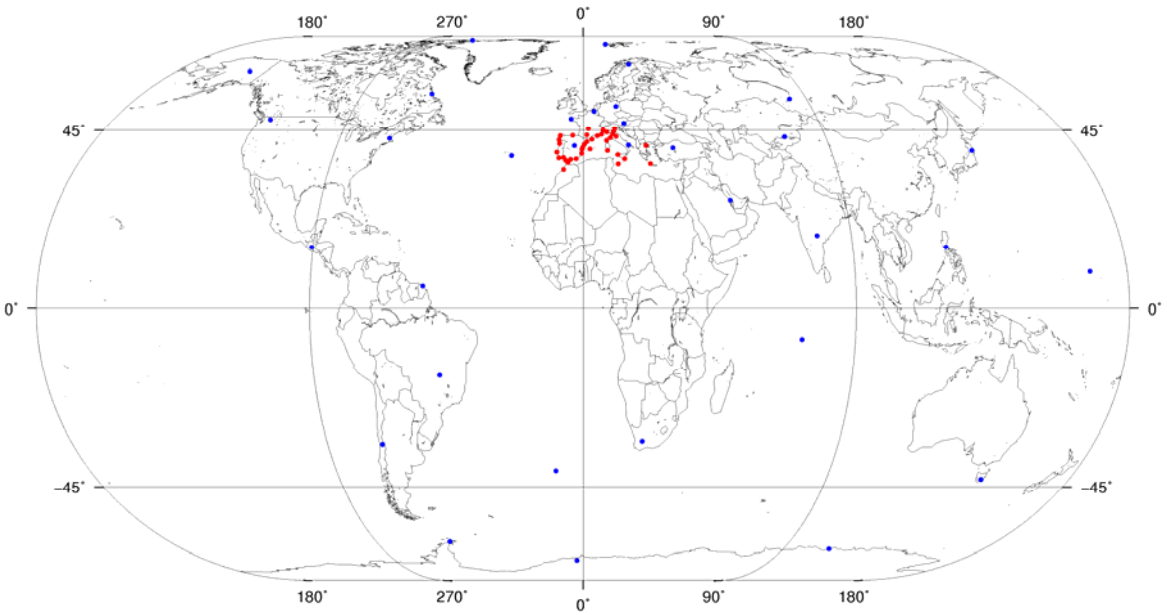

Fig.6 – IGS (blue) and EPN (red) stations used on UPorto GNSS solutions.

3.2.1.4 Data reduction to sea level

To be able to use the GNSS-derived tropospheric fields to correct altimeter measurements, the computed ZHD and ZWD have to be reduced to sea level by applying separate corrections for the two components. A procedure described by Kouba (2008) was used here for computing the correction for station height and is briefly summarized below.

The formula by Saastamoinen (1972) – later revisited by Davis et al. (1985) - provides high accuracy in the calculation of the hydrostatic delay solely based on surface pressure:

$$\mathrm{ZHD} = \frac{0.0022768\, p(h_s)}{1 - 0.00266\cos(2\phi) - 0.28 \cdot 10^{-6} h_s} \qquad (5)$$

where $p(h_s)$ is the surface pressure (in hPa), φ is the geodetic latitude, h_s is the surface height (at the station location) above the ellipsoid (in meters) and ZHD results in metres. The atmospheric pressure height dependence is modelled by

$$p(h_s) = p(h_0)\,(1 - 0.0000226 \cdot h_s)^{5.225} \qquad (6)$$

where $p(h_0)$ is the sea level surface pressure. From the Saastamoinen formula, $p(h_s)$ is derived and used to determine $p(h_0)$. Getting back to the first expression, ZHD is then derived for sea level.

For the height reduction of the zenith wet delay, the semi-empirical expression derived by Kouba (2008) is used:

$$\mathrm{ZWD}(h_s) = \mathrm{ZWD}(h_0) \cdot \exp\left[-(h_s - h_0)/2000\right] \qquad (7)$$

where $\mathrm{ZWD}(h_0)$, the zenith wet delay for sea level, is derived from $\mathrm{ZWD}(h_s)$ determined by GAMIT.

3.2.2 Accuracy of the extraction of ZWD from STD

The estimation of the Zenith Wet Delay (ZWD) from the Slant Total Delay (STD) obtained by GNS S receivers relies on the knowledge of the Zenith Hydrostatic Delay (ZHD). Therefore, the accuracy of the derived ZWD depends both on accuracy of the GNSS derive ZTD and on that of ZHD.

The accuracy of present ZTD from UPorto solutions (or from EUREF centers since November 2006) is about 3 mm (see section 3.3.2).

The ZHD is responsible for about 90% of the total path delay caused by the troposphere on the altimeter measurement of the two-way travel time from the satellite to the nadir sea level (e.g. Chelton et al. 2001). It varies slowly in space and time - typical scales of 100–1000 km and 3–30 h, respectively (Bosser et al. 2007). Although it is by far the largest range correction to be performed, with values ranging from around 2.25 m to 2.35 m, the estimation of the dry

tropospheric correction is accurately performed solely based on sea level pressure (980-1035 hPa) (Chelton et al. 2001) (e.g. by using the model developed by Saastamoinen (1972) and later refined by Davis et al. (1985) - equation (5) above).

Although the dry tropospheric correction is only moderately sensitive to errors in the surface pressure, a 5 hPa accuracy would be needed to secure a 1 cm accuracy (Chelton et al. 2001). When direct measurements of surface pressure are not available, ZHD estimations have to rely on pressure values derived from Numerical Weather Models (NWM) as those from ECMWF or NCEP (U.S. National Centers for Environmental Prediction).

The use of the modified Saastamoinen model together with NWM sea level pressure (e.g. ECMWF global 0.25°×0.25° grids generated every 6 hours) results in an uncertainty of less than 1 cm in the dry tropospheric range correction (Chelton et al. 2001). Recent studies (e.g. Bosser et al. 2007) further refined the Saastamoinen model by using an updated global Earth gravity model and a global climatology for air density (instead of the standard atmosphere of the original formulation). From the latter, it is claimed that an accuracy of 0.1 mm can be achieved for the dry correction providing surface pressure measurements can be guaranteed within an uncertainty of 0.1 hPa (requiring the use of high-accuracy barometers during quiet meteorological conditions, which does not usually happen).

Any improvement on the estimation of the dry tropospheric correction will also impact the quality of the GNSS-derived ZWD, as the latter is obtained by subtracting the hydrostatic component to the GNSS-derived total correction. A number of studies (e.g. Bai and Feng 2003, Hagemann et al. 2003 and Wang et al. 2007) have been conducted to assess the accuracy of the NWM-derived surface pressure for over-land GPS stations locations. A comparison of the accuracy of the NWM derived surface pressure with that obtained by collocated synoptic measurements for a set of land based GNSS stations can be found in Hagemann et al. (2003). Differences up to 3 hPa were reported by the authors to frequently occur, varying with station location and time of the year (significantly larger deviations were also found for some locations). Those differences did not present a specific and easy to model space- or time-pattern. As, unfortunately, only a very limited number of GNSS stations are equipped with meteorological sensors, Bai and Feng (2003) also stressed the need for seeking alternative sources for surface meteorological data or the use of solutions, which bypass the need for such data, if one wants to take advantage of the existing GNSS networks. Hagemann et al. (2003) refer a less than 1 hPa mean bias between collocated surface pressure measurements and those horizontally and vertically interpolated from nearby (up to a 100 km distance) World Meteorological Organization (WMO) stations. Wang et al. (2007) also found good results when using spatially and temporally interpolated synoptic surface pressure values from the 3-hourly WMO stations measurements.

Aiming to inspect the accuracy of the dry correction present on altimeter products, dry tropospheric correction values present at Envisat Geophysical Data Records (GDR) files (cycles 30 to 64 – September 2004 to December 2007) were compared with those derived from *in situ* surface pressure data at four GPS stations (GAIA, CASC and LAGO in the coast of Portugal and PDEL in the Azores Islands). Results show differences with a mean value of

[2 ± 3 (mm)] that range from -5 to 20 mm. In this analysis, only points within 100 km from each station and 50 km from the coast have been considered. Although the extreme values occur at ground-track points closer than 10 km from the coast, there is no clear degradation pattern associated with their distance to land.

Comparisons made at the same four GNSS stations (GAIA, CASC, LAGO and PDEL), for the period 2002-2007, where ZHD values were computed from local surface pressure data and from VMF1 grids, show an agreement within 3.4 mm accuracy (1-σ) for the ZHD computed at station height. Therefore, the corresponding wet correction (ZWD) can be separated from the dry correction (ZHD) with the same accuracy. This result is valid for the separation of the two components at station height. Due to error propagation, the corresponding errors at sea level are larger by a variable amount, depending on station height and on ZWD value and may increase by up to ~30%. However the corresponding error in ZTD is much smaller, since the errors in ZHD and ZWD have opposite signs and they almost cancel out.

These results show that VMF1 grids can be used to estimate ZHD at coastal stations with 4 mm accuracy. Therefore, ZWD can be separated from ZTD, computed for example at EUREF stations, with a\n error well below 1 cm. This result holds for stations near the coast, adequate for the purpose of this study, where the pressure fields do not suffer strong variations. At inland stations, far from the coast, it is found that the pressure fields may suffer seasonal variations that are not modelled in VMF1. In any case, the use of ECMWF 0.25°x0.25° grids, instead of the 2.0°×2.5° VMF1 grids will certainly improve the determination of ZHD and therefore the corresponding estimation of ZWD.

Considering the accuracy of ZWD determined at sea level, what is required for satellite altimetry, the above error analysis allow to conclude that, with present GNSS derived ZTD with 3 mm accuracy and ZHD computed from VMF1 at coastal stations with a 4 mm accuracy, the derived ZWD will have an accuracy of ~5 mm, in summary, bellow 1 cm.

3.3 Analysis of GNSS derived tropospheric fields and corresponding GDR fields

3.3.1 Analysis of the spatial variability of altimeter tropospheric fields

To analyse the spatial distribution of altimeter tropospheric corrections, maps of the mean and standard deviation of each field (ZHD and ZWD) for period A (September 2002 to August 2005) have been computed and are presented on Figures 7 and 8 for the whole world. To get a better idea of the variation of the same fields on the study region, Figure 9 represents an enlarged vision of these fields for the west European region. These maps show that ZHD and ZWD present different patterns of spatial variability. This is particularly clear in the global maps. Although the study region presents a relatively low variability, each tropospheric field still reveals specific spatial patterns. This information might be considered in the specification of the needs for adequate GNSS stations coverage for the computation of tropospheric corrections for coastal altimetry.

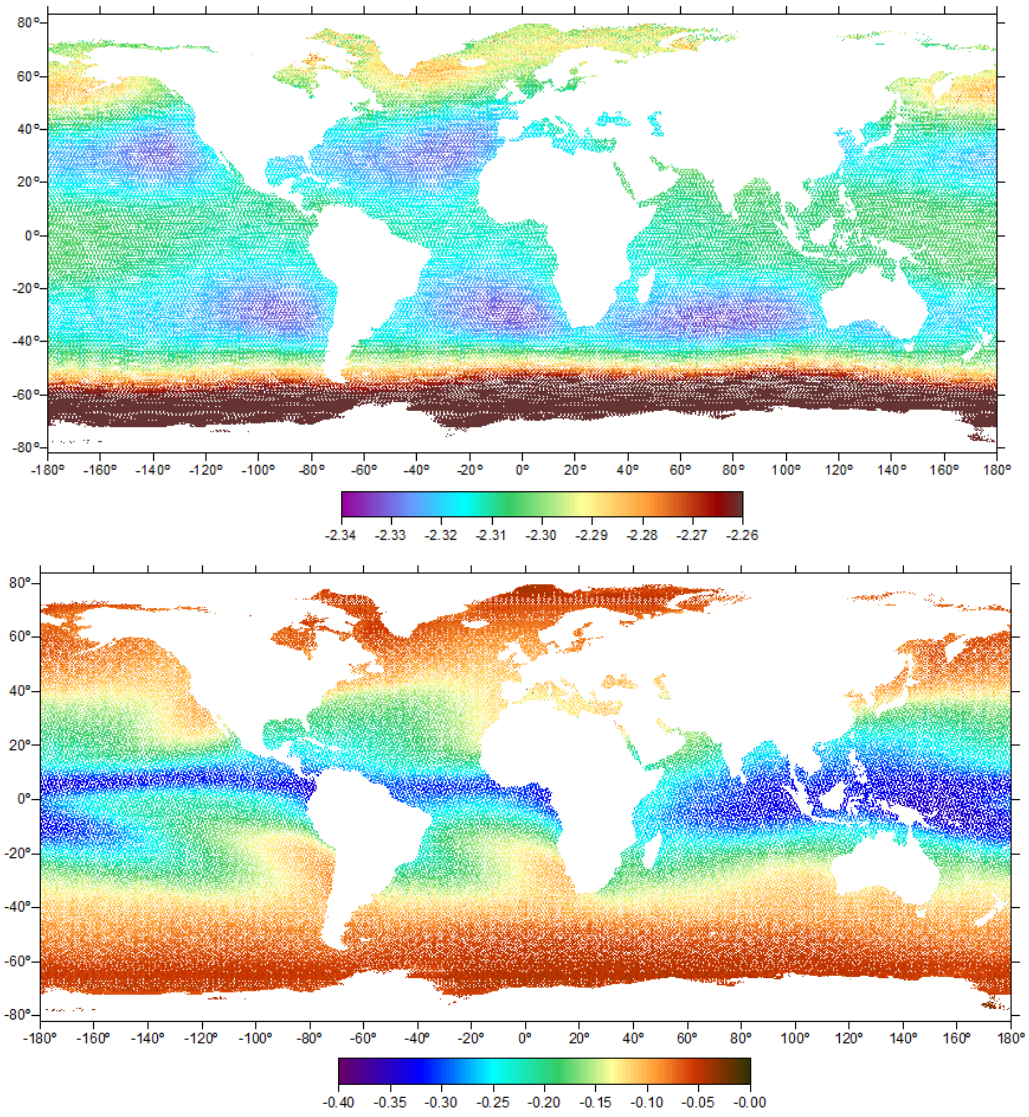

Fig.7 – For the whole world, mean values of ZHD (top) and ZWD (bottom) (in metres) for period A and 4 satellites: T/P, Jason-1, Envisat, GFO.

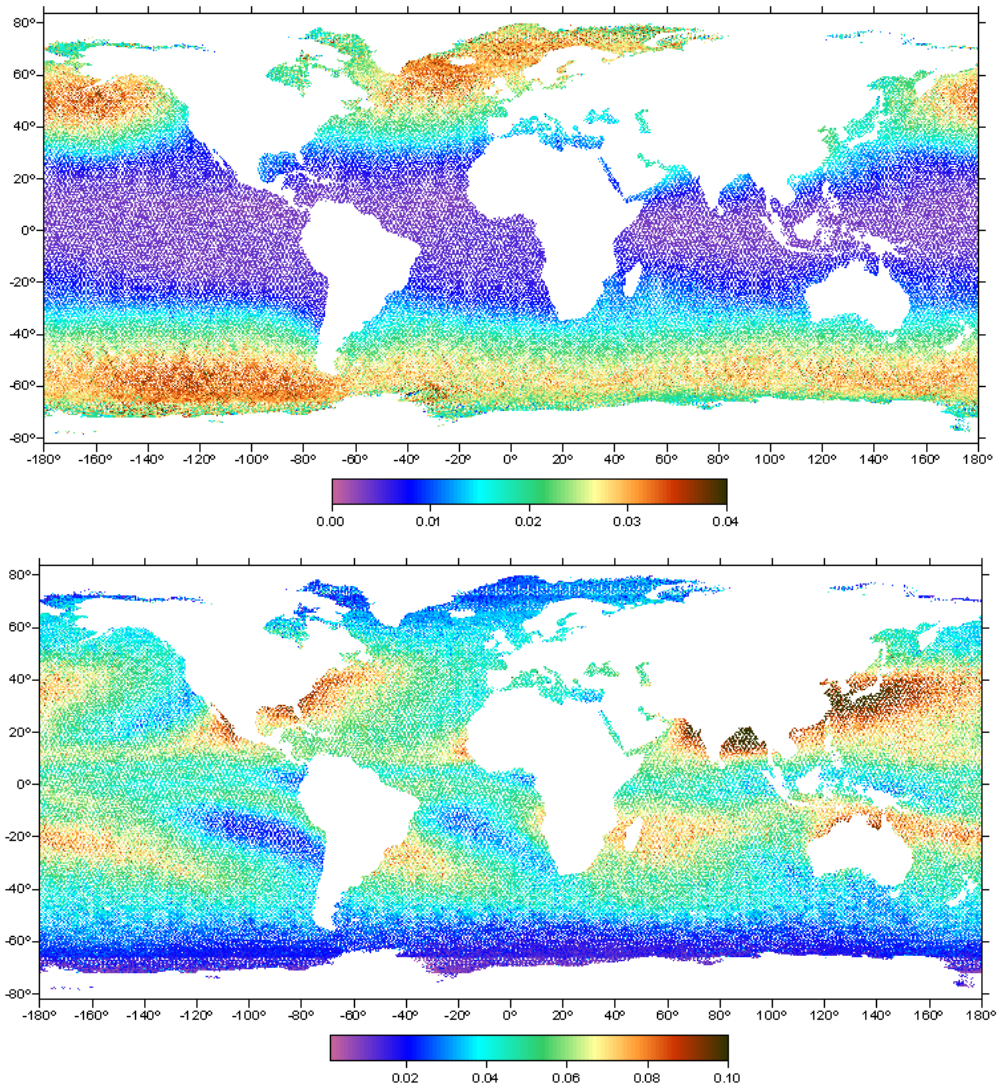

Fig.8 – From top to bottom, for the whole world, standard deviation of ZHD and ZWD (in metres), respectively, for period A and 4 satellites: T/P, Jason-1, Envisat and GFO.

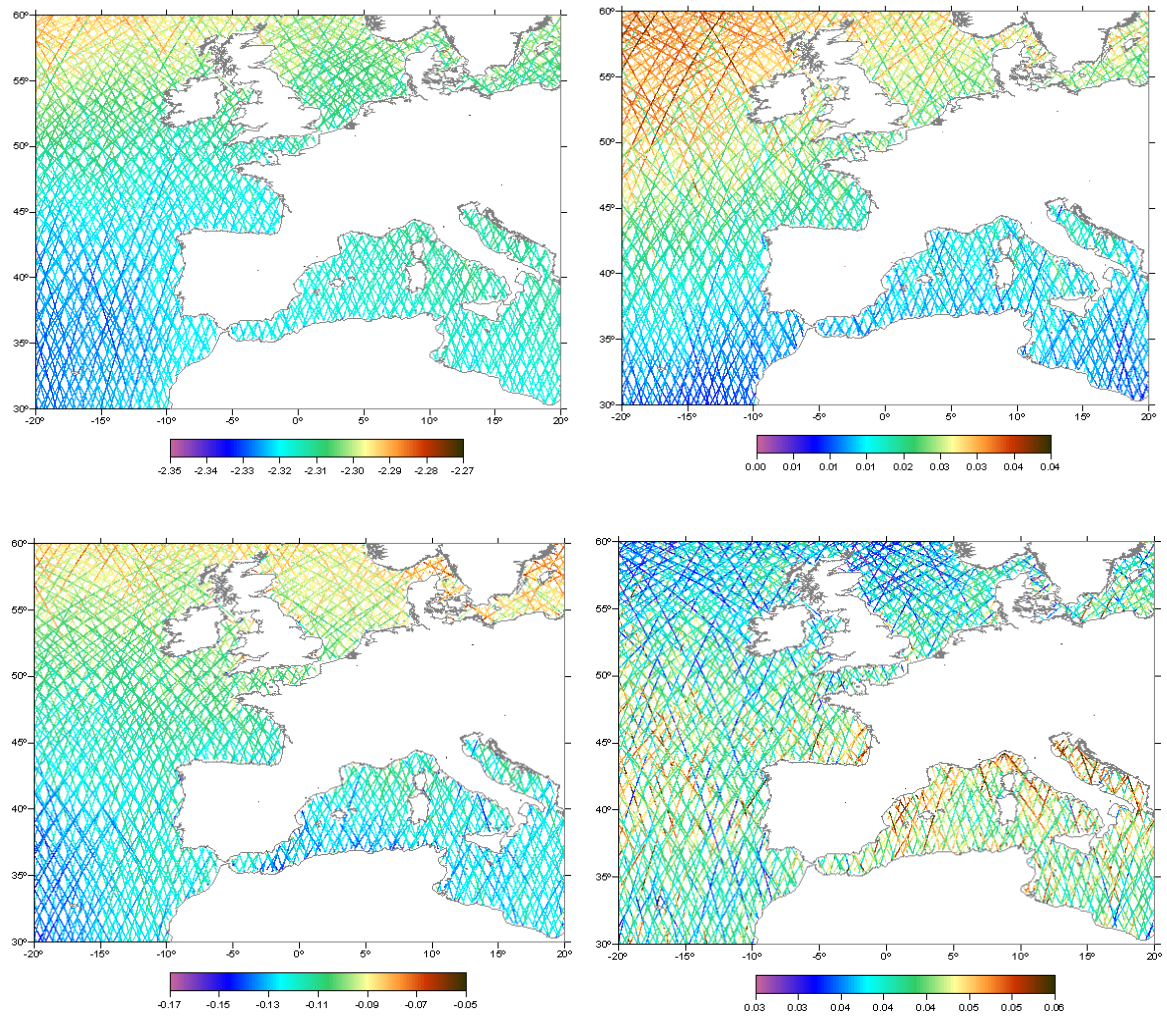

Fig.9 – From top to bottom, for the west European region, mean (left) and standard deviation (right) of ZHD and ZWD (in metres), respectively, for period A and 4 satellites: T/P, Jason-1, Envisat and GFO.

3.3.2 Comparison between GNSS derived tropospheric fields and corresponding fields present on GDRs.

With the purpose of inspecting the suitability of GNSS-derived tropospheric parameters for correcting coastal altimetry, a comparison study between two types of tropospheric fields has been performed and is presented here. These fields are the GNSS-derived tropospheric corrections (dry or ZHD and wet or ZWD) at a network of European stations near the coast and the corresponding altimeter tropospheric corrections, usually present on GDR products, at the nearby points with valid radiometer correction.

As mentioned aboved, the 3-year period of the analysis (Period A: September 2002 to August 2005) has been selected as the unique period for which there were four altimeter missions with different ground tracks: T/P, Jason-1, Envisat and GFO. GNSS data were available for the same period and for a network of 13 stations in the

West European region ($30° \le \varphi \le 55°$, $-20° \le \lambda \le 5°$): ZHD+ZWD from UPorto solutions, derived at 1 hour interval.

Altimeter tropospheric fields have been obtained from the RADS database or from AVISO, as described in section 1. ZHD is the dry correction from ECMWF or NCEP and ZWD is the wet MWR correction and altimeter data have been stacked. All statistics presented on tables 1 and 2 have been derived from RADS data. On the contrary, Figures 10 to 13 have been derived using AVISO data. This happens since RADS data were only available for this study at a later stage. And there was no time to update these figures also using RADS data. However, this does not affect the results, since the referred figures are only illustrative.

RADS data used in the subsequent statistics have been edited in such a way that only points with valid radiometer flag and valid MWR quality flag (for Envisat) were used. This results in a rejection of a large number of points near the coast which are present in the AVISO dataset.

For each point along each altimeter ground track, GNSS data of the surrounding stations have been interpolated for the altimeter measurement time. Therefore, for each altimeter point on the reference ground tracks, a set of time series of tropospheric fields have been generated: for the dry (ZHD) and wet (ZWD) altimeter tropospheric corrections and for the corresponding field determined at each GNSS station. One of the first results that came out of this study was the importance of correctly performing the height corrections to the GNSS tropospheric fields, since the parameters determined at each station refer to station height and must be correctly reduced to sea level for use in satellite altimetry. For ZHD the height correction is almost a bias, function of station height, and can reach several decimetres; for ZWD, although the correction is smaller (order of a few centimetres), it is a function of ZWD itself.

Various statistics have been computed for each pair of altimeter and station fields: correlation, mean and standard deviation (sigma) of the differences between the altimeter and the corresponding GNSS-derived field, for the nearest station (Tables 1 and 2) or for the station with maximum correlation (maps on Figures 10 to 13). Results for the NW Iberia are shown on Figures 10 and 11, for ZHD and ZWD, respectively and the corresponding results for the west Mediterranean on Figures 12 and 13.

Tables 1 and 2 show the statistics for the aforementioned fields and the whole study region ($30°\le\varphi\le55°$, $-20°\le\lambda\le5°$). Although points at larger distances have also been considered, in this statistical analysis only points up to 100 km distance of the GNSS station have been included (as for Jason-1 and T/P the number of altimeter ground-track points with valid radiometer measurement within the resulting area was very low, the limit was extended for these two satellites to a 150 km maximum distance to GNSS station to ensure the statistical significance of the results).

For the comparison between GNSS-derived and Envisat ZHD, the statistics for the mean difference between the two corrections are, in millimetres, -2.7, 5.7, 1.0 and 2.1 for minimum, maximum, mean and standard deviation, respectively. The corresponding statistics for ZWD are -12, 17, 4.2 and 5.9 (in mm).

These values are a clear indication of the agreement between the altimeter and GNSS-derived fields.

Tab.1 - Statistics of the comparison (altimetry-GPD) of sea level ZWD time-series for altimetry track points (number in brackets) distant up to 100 km (Envisat and GFO) or 150 km (Jason-1 and T/P) from nearest GNSS station (difference and sigma in mm).

		min	max	mean	sigma
Envisat (524)	Difference	-12	17	4.2	5.9
	Correlation	0.747	0.988	0.926	0.042
	Sigma	8.2	30.2	17.1	3.9
Jason-1 (286)	Difference	-15.4	33.9	5.1	6.5
	Correlation	0.684	0.970	0.894	0.044
	Sigma	14.0	40.4	22.0	4.3
T/P (308)	Difference	-20.5	9.4	-1.3	5.4
	Correlation	0.743	0.974	0.916	0.040
	Sigma	12.2	36.5	19.1	4.1
GFO (455)	Difference	-123.6	4.8	-10.7	10.6
	Correlation	0.702	0.989	0.928	0.041
	Sigma	7.4	32.2	17.8	4.1

Tab.2 - The same as Table 1 for ZHD.

		min	max	mean	sigma
Envisat (524)	Difference	-2.7	5.7	1.0	2.1
	Correlation	0.905	0.998	0.976	0.023
	Sigma	0.9	7.3	2.9	1.4
Jason-1 (286)	Difference	-5.2	10.2	1.0	2.5
	Correlation	0.851	0.994	0.977	0.018
	Sigma	1.2	6.5	3.1	0.9
T/P (308)	Difference	-2.9	4.5	0.1	2.1
	Correlation	0.926	0.997	0.980	0.012
	Sigma	1.3	7.7	2.9	0.9
GFO (455)	Difference	-3.1	4.0	0.3	1.9
	Correlation	0.858	0.999	0.970	0.037
	Sigma	1.0	7.0	3.0	1.4

Overall, the results show that for ZHD the correlations are high (typically around 0.98) for all four satellites (slightly lower for GFO). For ZWD, correlations between altimeter and GNSS are 0.93 for Envisat and GFO (distances up to 100 km) with lower values for T/P (0.92) and Jason-1 (0.89), for which points up to 150 km have been considered. For ZHD (Table 2), the mean difference is below 1 mm and the mean standard deviation of the differences has values around 3 mm for all missions. For ZWD (Table 1), although for all satellites except GFO the absolute mean difference is below 1 cm, actual values depend on the mission: around 4 mm for Envisat, 5 mm for Jason-1, -1 mm for T/P and -11 mm for GFO. The mean standard deviation of the differences presents values from 17 to 22 mm for all satellites, which is within the expected variability for this field.

The results show that, as expected, as the distance to the station decreases, the correlations increase and the mean and sigma of the differences decrease in a consistent way.

The station showing maximum correlation with each altimeter track point is, in general, one of the closest stations, not necessarily the closest one, due to local variations of the atmospheric fields, as shown in the top right map on Figs 10 to 13.

The top left maps on Figures 10 and 12, showing the percentage of valid cycle points for the study period, allows understanding why for some close-to-land tracks the maximum correlation occurs for a station which is not in the vicinity of the point. In these cases, the time series have a small number of points and, therefore, the corresponding correlations are not statistically significant. This is clear for the ascending 917 Envisat track almost parallel to the NW Spanish coast (percentage of valid cycle points below 30%). Note that if these maps were generated with RADS data, there would be no data at all for this short distance to land, as all those points would have been edited out).

When comparing the two fields (ZHD and ZWD), the highest correlations and the smallest differences are shown for ZHD since this field is easier to model and suffers the smallest variations; on the contrary, ZWD reveals the lowest correlations and the highest differences as it undergoes the largest spatial and temporal variations.

In face of the results, the different values for the mean differences in the ZWD field suggest that there may be a bias or scale factor between GFO MWR and the microwave radiometers of the other satellites. In particular, Envisat and Jason-1 datasets seem to be very consistent.

RADS altimetry are known to be well calibrated, with state-of-art corrections for all known drifts, biases, scale factors and any other irregularities detected on data. In spite of this, due to the different footprint length, Envisat and GFO show points at distance to the coast up to 20 km while for Jason-1 and T/P all points up to 50 km are rejected. Therefore, a precise comparison between the various missions solely based on the comparison with the GNSS data is difficult to achieve.

This study shows the suitability of the GNSS-derived tropospheric fields for use in the correction of the coastal altimeter measurements. However, due to the relatively scarce number of GNSS stations, these fields have to be combined with additional available data to obtain the required spatial information.

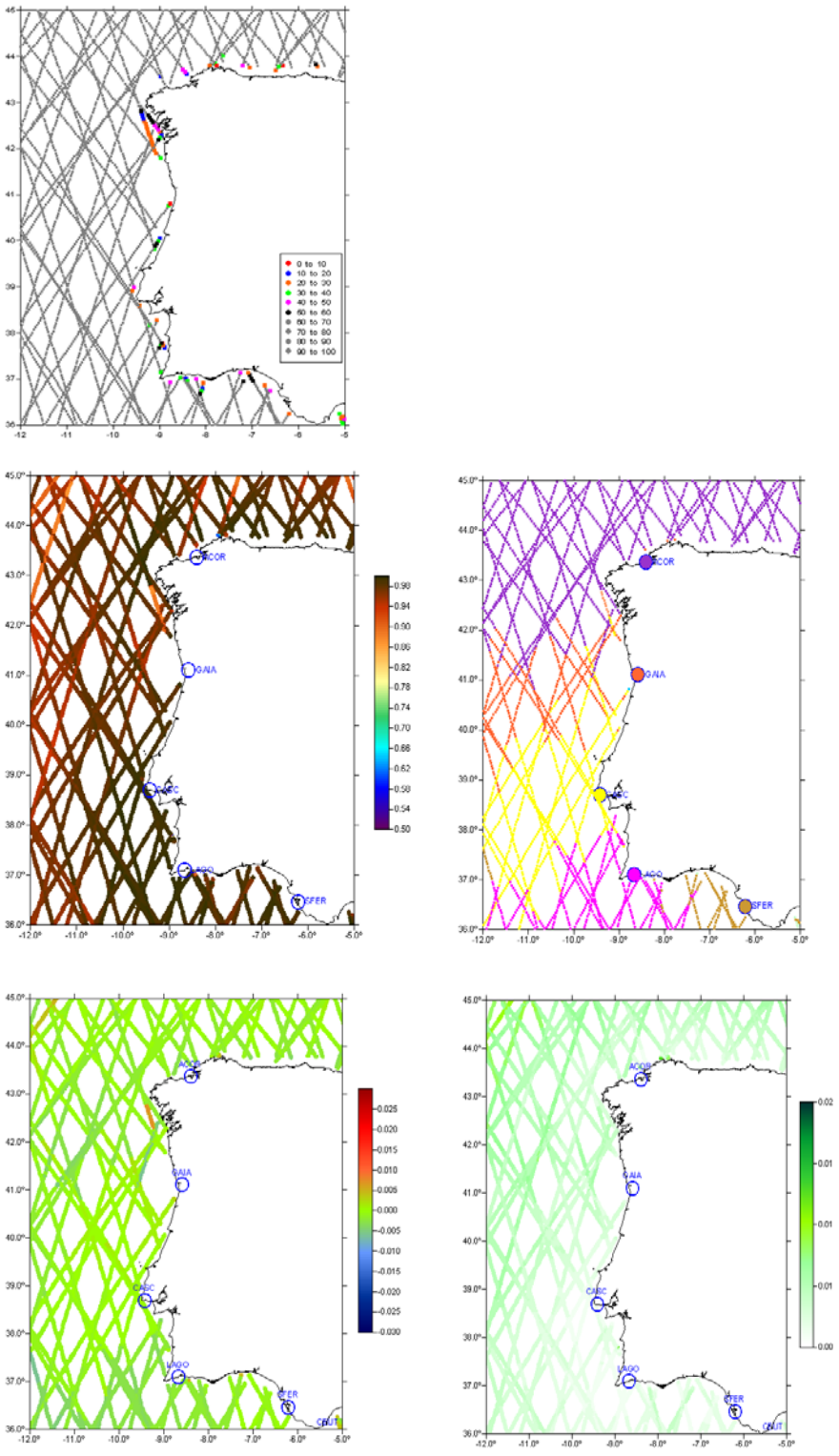

Fig.10 - From top to bottom and left to right: percentage of valid cycle points, maximum correlation, station for which the correlation is maximum, mean and standard deviation of the differences between altimeter ZHD and GNSS derived ZHD (in metres) for the station with maximum correlation. Results refer to UPorto solutions for period A and the NW Iberian region. GNSS fields have been corrected for station height.

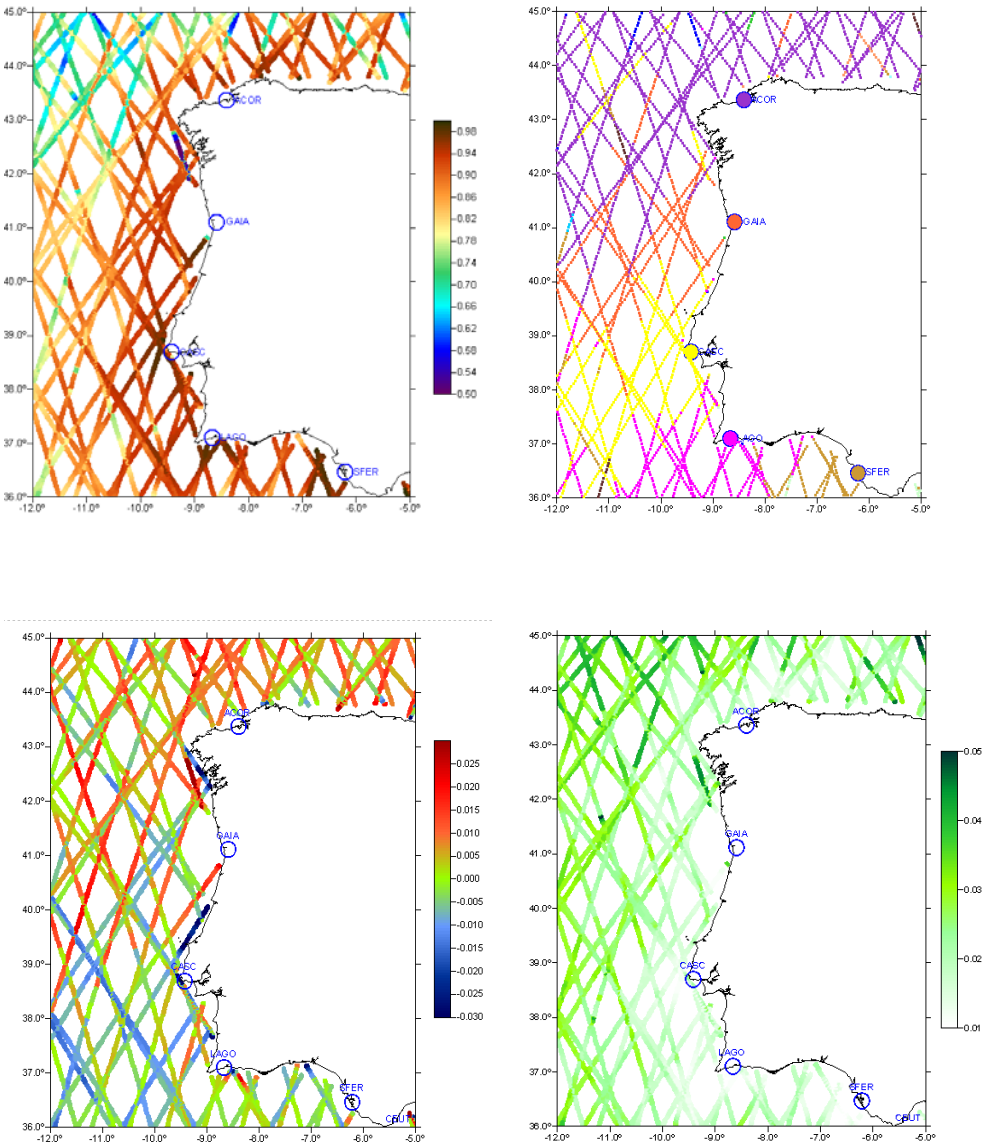

Fig.11 - From top to bottom and left to right: maximum correlation, station for which the correlation is maximum, mean and standard deviation of the differences between altimeter ZWD and GNSS derived ZWD (in metres) or the station with maximum correlation. Results refer to UPorto solutions for period A and the NW Iberian region. GNSS fields have been corrected for station height.

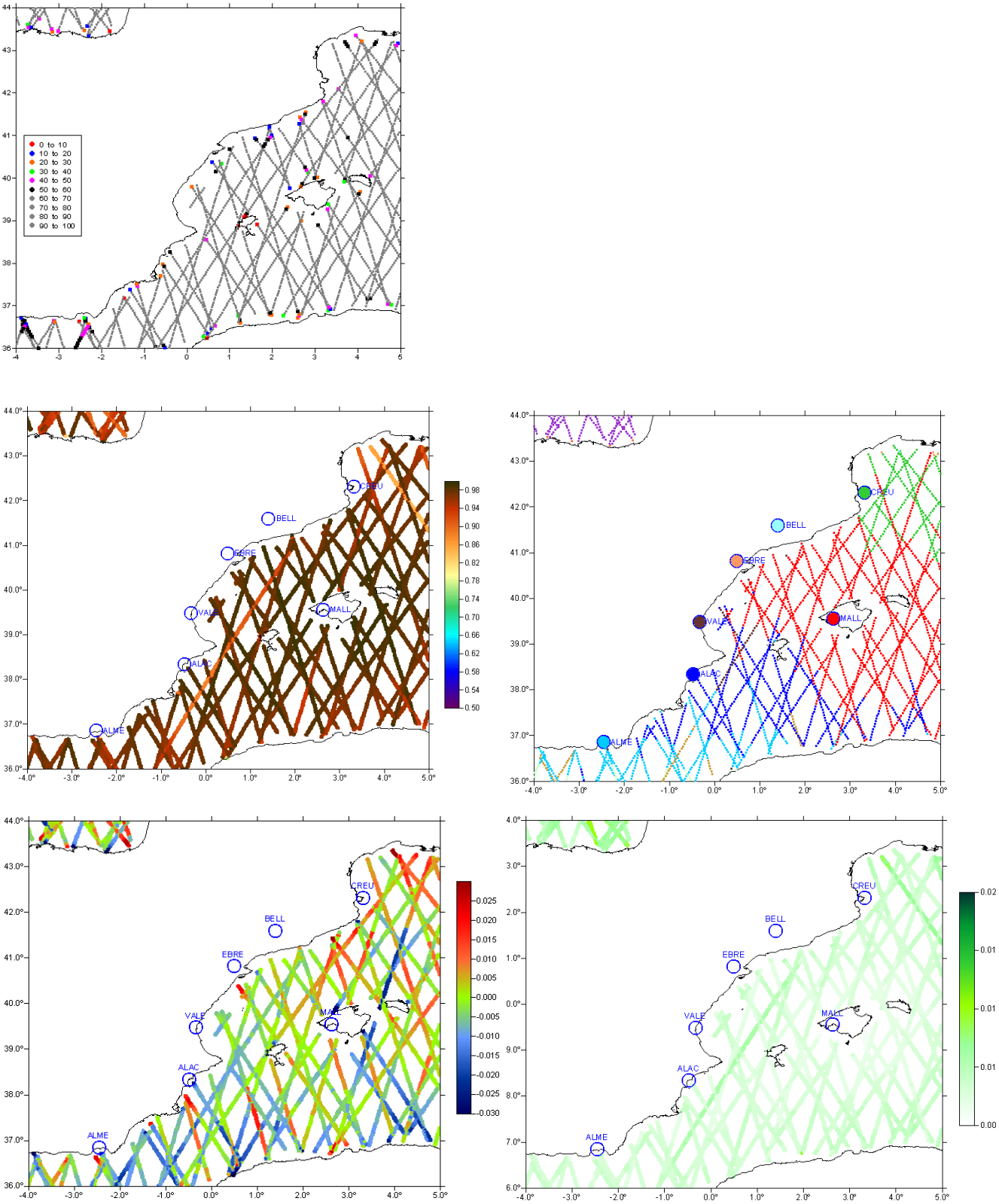

Fig.12 - From top to bottom and left to right: percentage of valid cycle points, maximum correlation, station for which the correlation is maximum, mean and standard deviation of the differences between altimeter ZHD and GNSS derived ZHD (in metres) for the station with maximum correlation. Results refer to UPorto solutions for period A and the West Mediterranean region. GNSS fields have been corrected for station height.

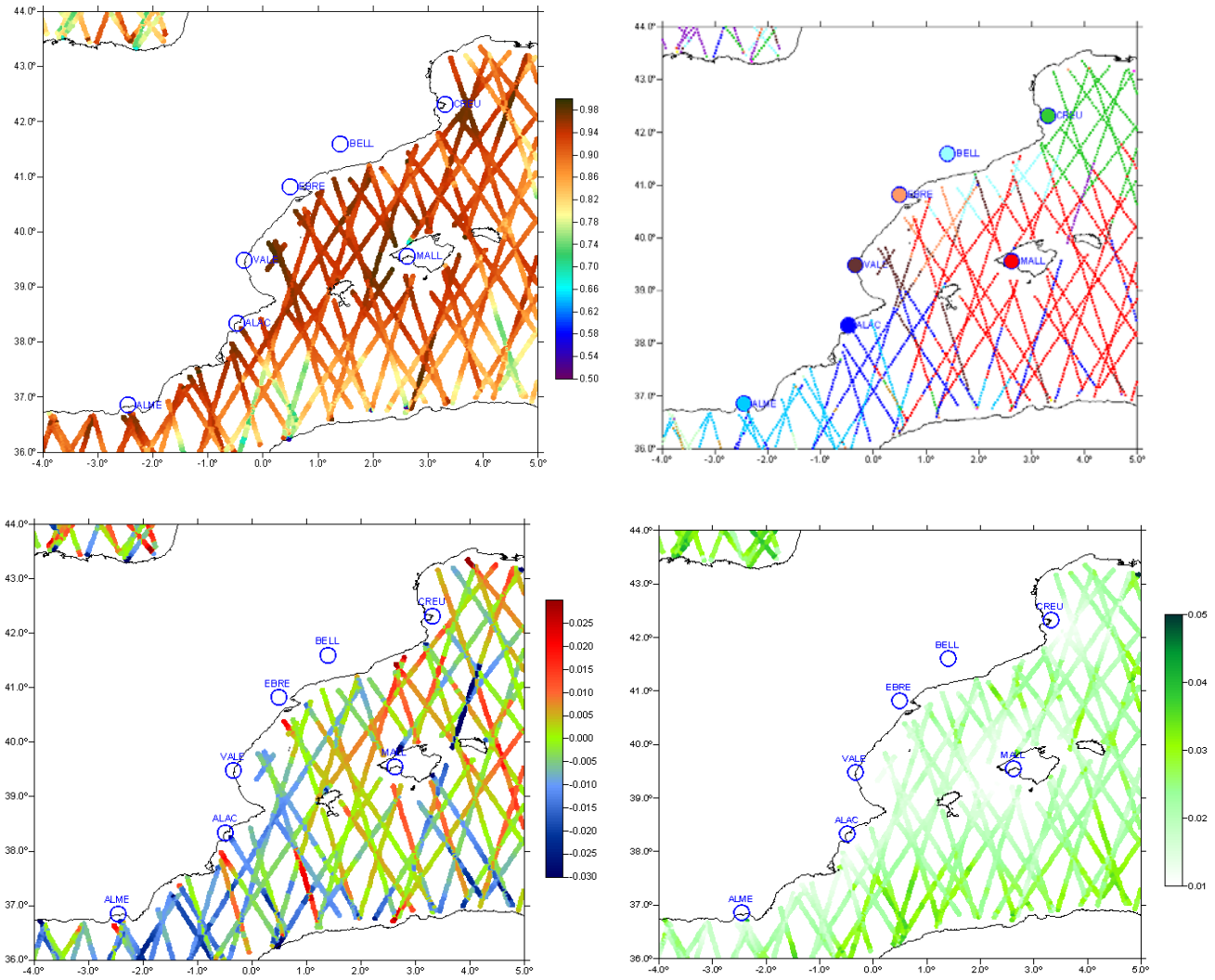

Fig.13 - From top to bottom and left to right: maximum correlation, station for which the correlation is maximum, mean and standard deviation of the differences between altimeter ZWD and GNSS derived ZWD (in metres) for the station with maximum correlation. Results refer to UPorto solutions for period A and the West Mediterranean region. GNSS fields have been corrected for station height.

3.3.3 Effect of Height reduction on GNSS derived tropospheric fields.

The effect of the reduction of the GNSS-derived tropospheric fields to sea level has already been highlighted in the comparison study between altimeter and GNSS-derived fields for period A (September 2002 to August 2005). Furthermore, for a longer period (period B: 2002-2007), a comparison is now presented between non height-corrected and height-corrected UPorto GNSS-derived fields. Plots on Figure 14 show UPorto ZTD, ZHD and ZWD, before (in red) and after (in green) applying height correction for GAIA (h=232 m) and BELL (h=803 m) stations. These plots illustrate well the importance of the height correction. For ZHD the height correction is almost a bias, function of station height, and can reach several decimetres, as is the case of BELL station, for which the mean correction reaches

212 mm, while for ZWD the correction is smaller, function of ZWD itself, and can reach several centimetres (mean correction is 43 mm for the same station). Plots on Figure 15 better illustrate these effects, for a shorter period of time.

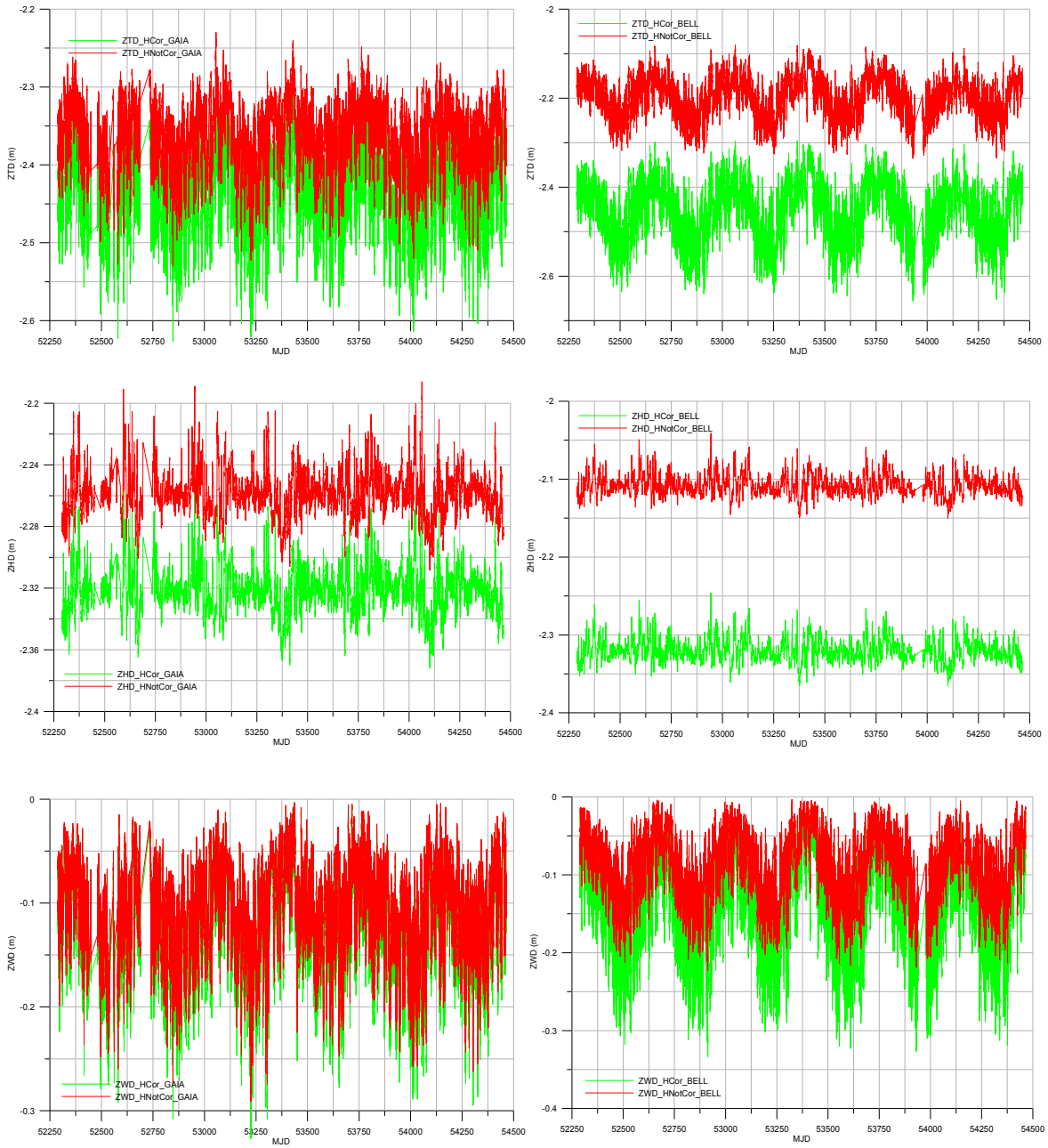

Fig.14 – From top to bottom, UPorto height corrected (green) vs. non height corrected (red) ZTD, ZHD and ZWD for GAIA (left, h=232m) and BELL (right, h=803m), for the period 2002-2007.

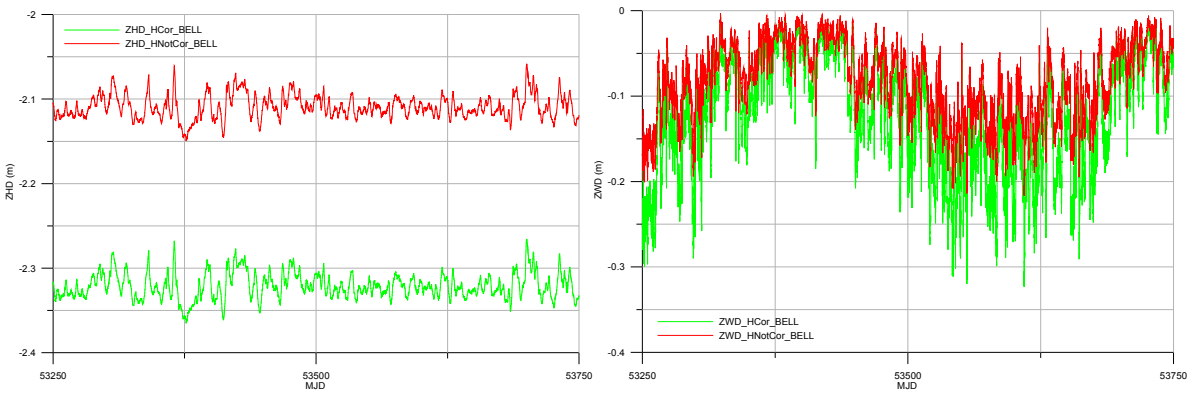

Fig.15 - UPorto height corrected (green) vs. non height corrected (red) ZHD (right) and ZWD (left) for BELL station, for a 500-day period.

3.4 Comparison between UPorto and EUREF ZTD solutions

Aiming at the comparison between UPorto and EUREF solutions, the differences between UPorto and EUREF station-height derived ZTDs, for the whole set of 13 stations and period B (2002-2007), have been analysed. For all stations and for this period (568732 data values), the statistics of the differences are, in mm, -68.2, 259.1, 6.7 and 6.8 for minimum, maximum, mean and standard deviation, respectively.

For most of the stations the pattern of the differences is similar to Figure 16 which shows the results for CASC (Cascais, Portugal). The differences show an irregular pattern, with higher differences at the beginning and various discontinuities during this period. These discontinuities are related to changes in the processing adopted at the EUREF centres. In contrast, UPorto solutions have been derived using a uniform methodology for the whole period.

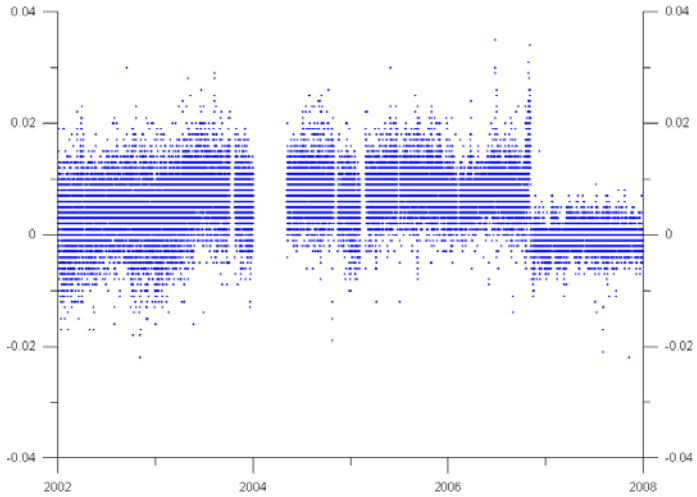

Fig.16 – Differences between UPorto and EUREF ZTD (in metres), without height correction, for CASC GNSS station (period 2002-2007).

A major change in the EUREF processing occurred in November 5, 2006, after which the differences, for all 13 stations become uniform and reduce to the values presented in the last row of Table 3, which presents, for the various stations, the differences (UPorto - EUREF) for the period from 5-Nov-2006 to 31-Dec-2007. The sigma value of 3.1 mm, obtained for the last period, should be a realistic indicator of the accuracy of UPorto GNSS solutions, considering that these solutions are derived using state-of-the-art mapping functions.

Tab.3 – Statistics: minimum, maximum, mean and standard deviation of the differences between UPorto and EUREF ZTDs, not corrected for station height for the period (2006 November 5 -2007 December 31).

	UPorto ZTD – EUREF ZTD (Height not corrected)			
GNSS st. (nvalues)	min (mm)	max (mm)	mean (mm)	sigma (mm)
ACOR (8826)	-10.1	33.4	0.4	2.5
ALAC (10046)	-18.7	27.6	0.1	2.7
ALME (9069)	-26.1	18.9	0.0	3.4
BELL (9262)	-26.5	23.8	-0.1	2.9
CASC (9924)	-22.2	14.6	-0.5	2.2
CEUT (142)	-16.7	28.2	-0.7	6.2
CREU (9096)	-12.9	24.5	2.8	2.7
EBRE (8946)	-15.9	22.5	-0.4	2.6
GAIA (9986)	-23.4	17.3	0.3	2.6
LAGO (9844)	-11.6	10.6	-0.4	2.4
MALL (10032)	-36.0	13.8	-3.5	3.8
SFER (9904)	-19.0	30.2	-0.3	2.4
VALE (8942)	-12.2	22.5	-1.4	2.8
All (114019)	-36.0	33.4	-0.3	3.1

3.5 Data combination

3.5.1 Objective Analysis

A linear space-time objective analysis (OA) technique that makes use of wet delay estimates from different sources and takes into account the data measurement noise has been implemented to generate reliable wet tropospheric correction (delay) (ZWD) estimates at the satellite ground-track positions with invalid radiometer corrections. The theoretical formulation of the estimator and associated error is given in Bretherton et al. (1976).

The technique combines independent available ZWD values derived from ECMWF model atmospheric fields, from the GNSS stations and from the microwave radiometer measurements (only valid measurements) to update a first guess value known *a priori* at each altimeter ground-track location with invalid radiometer measurements. The statistical technique interpolates the wet correction measurements at the latter locations and epochs from nearby (in time and space) independent measurements and provides the quantification of the interpolation errors by taking into account the respective accuracy of each data set. Therefore, different observations are weighted according to statistical information regarding their errors. The combination of ZWD rather than ZTD independent quantities is preferred, since, as described before, the dry (hydrostatic component, ZHD) can be accurately derived from independent sources.

The technique also requires *a priori* information regarding the statistics of signal and noise variability and, given these parameters, estimates are optimal in the sense that no more accurate linear combinations of the observations, based on a least squares criterion, exist (Bretherton et al. 1976). Spatial covariances between each pair of observations and each observation and the location at which an estimate is required can be derived from a Gauss-Markov function (Schüler 2001), providing that the spatial correlation scale is known. To take into account the time variability of the ZWD field, an interpolation in time is also required and, therefore, the space-time correlation function shall be obtained by multiplying the space correlation function by a stationary Gaussian decay. Bosser et al. (2007) refer that the ZWD varies spatially and temporally with typical scales of 1 to 100 km and 1 to 100 minutes, respectively, and these ranges allow a preliminary establishment of the spatial and temporal correlation scales. More accurate estimates of the correlation scales can be obtained by the fitting of the empirical auto-covariance function.

The following datasets are to be merged together: wet corrections (ZWD) from MWR on-board altimetry missions (provided in GDR products) which, along the satellite ground-track, are flagged as ocean (valid radiometer flag), assumed simultaneously acquired; wet corrections (ZWD) derived from ECMWF or local/regional atmospheric models, provided at a regular grid spacing (preferably smaller than 0.25º) and with a desirable maximum 3-hour temporal sampling; the ZWD values derived at the GNSS stations. The latter estimates are, generally, derived from land-based stations and therefore the correction for station height should be applied; emphasis should be given to the merging of data derived from offshore stations (e.g. buoys and oil platforms), if available.

3.5.2 ECMWF-derived ZWD

The zenith wet delay (ZWD) at a radio receiver is known to be nearly proportional to the precipitable water - the vertically integrated water vapour overlying the receiver, PW – (e.g. Askne and Nordius 1987). This fact has enforced the use of GNSS stations for climate studies, allowing the integrated water vapour (IWV) to be derived from the zenith wet delay.

Based on the same assumption, within the focus of the present study, ECMWF Deterministic Atmospheric Model IWV data (total column water vapour, TCWV)

will be used to derive an over-ocean ZWD data set, to be merged to over-land GNSS-derived ZWD.

The dimensionless ratio of zenith wet delay (ZWD) and integrated water vapour (IWV) is (Askne and Nordius 1987):

$$\frac{ZWD}{IWV} = 10^{-6} \cdot R_W \cdot \left(k_2' + \frac{k_3}{T_M} \right) \quad (8)$$

where R_w is the specific gas constant for water vapour, T_M (in K) is the mean temperature of the troposphere (weighted by water vapour pressure, Davis et al. 1985) and k_2' = [22.1 ± 2.2] (K/hPa) and k_3 = [370100 ± 1200] (K^2/hPa) (Bevis et al. 1994) are constants derived from the atmospheric refractivity formula (e.g. Smith and Weintraub 1953). The constants needed for the conversion of ZWD into PW or IWV are known with sufficient accuracy, but the mean temperature of the troposphere has to be determined as well.

Several models, either local or global, have been developed which allow the estimation of T_M from the atmospheric surface temperature T_0 (e.g. Bevis et al. 1992, Bevis et al. 1994). The global model proposed by Mendes et al. (2000)

$$T_M = 50.4 + 0.789 T_0 \quad (9)$$

was derived via 50 radiosonde stations over a one-year period and will be used here to estimate the mean atmospheric temperature from surface temperature. According to Bevis et al. (1992), the relative error in the ZWD/IWV conversion factor is, to a very good approximation, that of T_M. Within this approach, ECMWF Deterministic Atmospheric Model surface temperature data (2-metre temperature, 2T) will be used for T_0.

3.5.3 Implementation of the methodology

A radiometer measurement has been considered invalid whenever the radiometer land-ocean flag (GDR field number 145) is set to 1 (land-flagged) or the MWR quality interpolation flag (GDR field number 146) is larger than 0 (the most comprehensive case). Both flags are given in the altimetry GDR product. For these measurements, an estimation of the wet delay with an associated error is output by the methodology. The observations include valid microwave radiometer measurements (for these, both the above-mentioned flags are equal to 0) and GNSS- and model-derived wet delay estimates. Altimetry- and model-derived observations are assumed to have the same white measurement noise of 1 cm, while a value of 5 mm was assigned to white noise of the GNSS-derived estimates.

In the absence of the knowledge of an empirical covariance model of the background field, a covariance function F(r) that decreases exponentially with the square of the distance between acquisitions was adopted:

$$F(r) = e^{-\frac{r^2}{C^2}} \quad (10)$$

where r is the distance between each pair of points and C is the spatial correlation scale. The correlation spatial scale assumes that the field is isotropic and has been set to 100 km (Bosser et al. 2007).

The temporal variability of the field is also taken into account and the covariance function is therefore represented by a space-time analytical function $G(r,\Delta t)$ that is obtained by multiplying the space correlation function F(r) by a stationary Gaussian decay of the form:

$$D(\Delta t) = e^{-\frac{\Delta t^2}{T^2}} \quad (11)$$

where Δt is the time interval between the acquisition of the measurements associated to each pair of locations and T is the temporal correlation scale, set to 100 minutes (Bosser et al. 2007). Both the temporal and spatial correlation scales are, at this stage, assumed to remain constant over the study region.

The covariance matrix between all pairs of observations and the covariance vector between the quantity under estimation and the measurements are computed from $G(r,\Delta t)$ to within the signal variance. The function G is normalized so that the correlation equals unity when r=0 and Δt=0.

Since the observations have quite different spatial and temporal samplings, some issues must be addressed in the data selection criteria. From the available observations for the merging procedure, only those that are contained in the influence region centred at the point where the estimation is to be performed and with radius equal to the space correlation scale are selected. This limits the number of model-derived observations selected for the OA, which otherwise would lead to their overweighting in the interpolation. Given that the temporal sampling of the ECMWF model is 6 hours, the temporal influence interval has been set to 3 hours to guarantee that, at least, one model sample grid contributes to the estimation of the background field.

Wet delay estimates from the GNSS stations are derived hourly. Results are presented considering wet delay estimates from GNSS that have been previously interpolated to a 30-minute interval.

Finally, valid microwave radiometer measurements contained in the spatial influence region and temporal interval are selected. With the data selection constraints aforementioned, these valid MWR measurements belong to the same pass as the invalid MWR measurements where an estimation of the field is required.

For each invalid MWR measurement, a first guess value has been computed as the mean value of the selected observations. The OA procedure updates this value with the information added by the measurements themselves.

Only measurements with altimeter land-ocean flag (GDR field number 144) set to zero are extracted from the GDR product.

In order to compute the noise-to-signal ratio to set up the covariance matrix, the *a priori* knowledge of the signal variance is required. Consequently, and at this stage, the data combination routine has been applied assuming a constant

variability of 4 cm RMS for the whole study region, with the uncorrelated errors and the data selection criteria above described.

At a next stage, the mapping routine shall be run again merely to generate realistic relative mapping error values, using the signal variance calculated, at the current stage, for the locations where the MWR measurements are persistently contaminated.

3.5.4 Results

The results presented here are based on the observations contained in Envisat Cycle 58 (from 07-05-2007 to 11-06-2007). Figure 17 shows the location of both valid (in blue) and invalid (in red) MWR measurements (i.e., those with radiometer land-ocean flag equal to 1 MWR quality interpolation flag larger than 0) for the region $30°\leq \varphi \leq 55°N$, $20W°\leq \lambda \leq 20°E$. Also shown in the figure is the location of the GNSS stations from which ZWD measurements were used in the data combination methodology. The correction for station height has been applied on the GNSS-derived ZWD values, previously to their merge, during the data combination methodology, with data from other sources.

The output of the data combination methodology is an estimation of the ZWD field for the location and time of each invalid MWR measurement. Each estimation has associated a relative error variance which, for Envisat Cycle 58, that is shown in Figure 18 (unit is percentage of the signal variance, assumed constant for the whole region and equal to 4 cm RMS). The error variance associated with the estimation decreases considerably when MWR and GNSS-derived ZWD measurements are available within the spatial and temporal influence regions. In general, ZWD estimations along the coastal regions have an error variance that does not exceed 30% of the signal variance.

In order to compute realistic error variances, the ZWD variability must be known *a priori*, as already mentioned. As an example, the ZWD variability for the period corresponding to Envisat Cycle 58 is shown (in m^2) in Figure 19: the top panel shows the signal variability computed using the ZWD estimates output from the data combination methodology, whereas the bottom panel shows the ZWD variability considering, for the period, the ECMWF-derived ZWD grids (one grid each 6 hours). In order to achieve the signal variability represented in the topmost panel of Figure 19, the data combination methodology was used to update the ZWD values of each ECMWF grid, when data from GNSS stations and MWR were available, according to the data selection criteria previously described. The spatial and temporal correlation scales have been set as 100 km and 3 hours, respectively.

From the example shown, despite the short time period for which the signal variability has been computed, it is noticeable the improvement in the signal variability, particularly in the vicinity of the coastal GNSS stations.

Hereafter, a detailed analysis of the results achieved for the Portuguese coastal region (using GNSS data from the Portuguese land-based GNSS stations) is presented. Figure 20 shows the results obtained for Envisat pass number 1, between latitudes 36º and 44ºN (ascending pass). The location of the

microwayve radiometer observations is shown in Figure 21: the blue dots represent valid MWR observations, whereas the red dots represent those flagged as invalid according to the criteria previously described. Wet delay estimates have been calculated for the locations and epochs of invalid measurements only. Also shown in Figure 21 are the locations of the GNSS stations along the Portuguese coast that provided data for this study. Those closer to the locations of pass 1 invalid measurements are Cascais (CASC, green circle) and Lagos (LAGO, cyan circle) stations.

Figure 20 shows the results obtained for Envisat pass number 1, between latitudes 36º and 44ºN (ascending pass). The location of the microwave radiometer observations is shown in Figure 21: the blue dots represent valid MWR observations, whereas the red dots represent those flagged as invalid according to the criteria previously described. Wet delay estimates have been calculated for the locations and epochs of invalid measurements only. Also shown in Figure 21 are the locations of the GNSS stations along the Portuguese coast that provided data for this study. Those closer to the locations of pass 1 invalid measurements are Cascais (CASC, green circle) and Lagos (LAGO, cyan circle) stations.

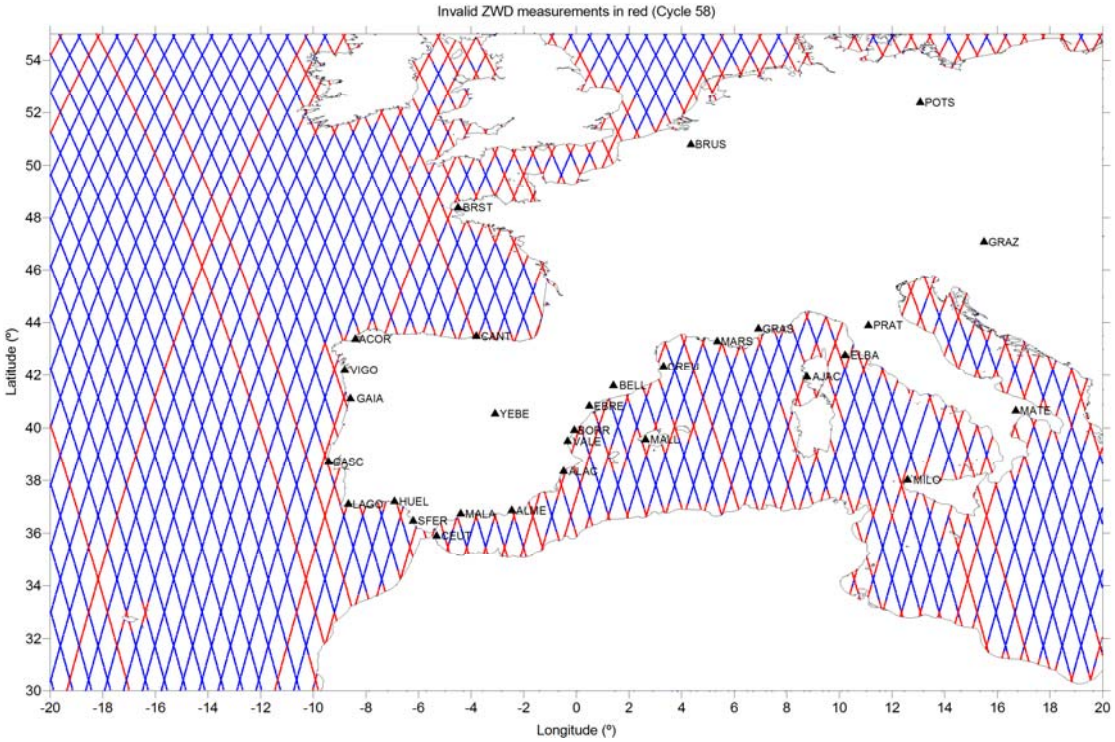

Fig.17 – Invalid MWR measurements for Cycle 58 shown (in red). Also shown is the location of the GNSS stations from which ZWD measurements were considered in the data combination methodology. Black triangles show the location of the GNSS stations used in the data combination methodology.

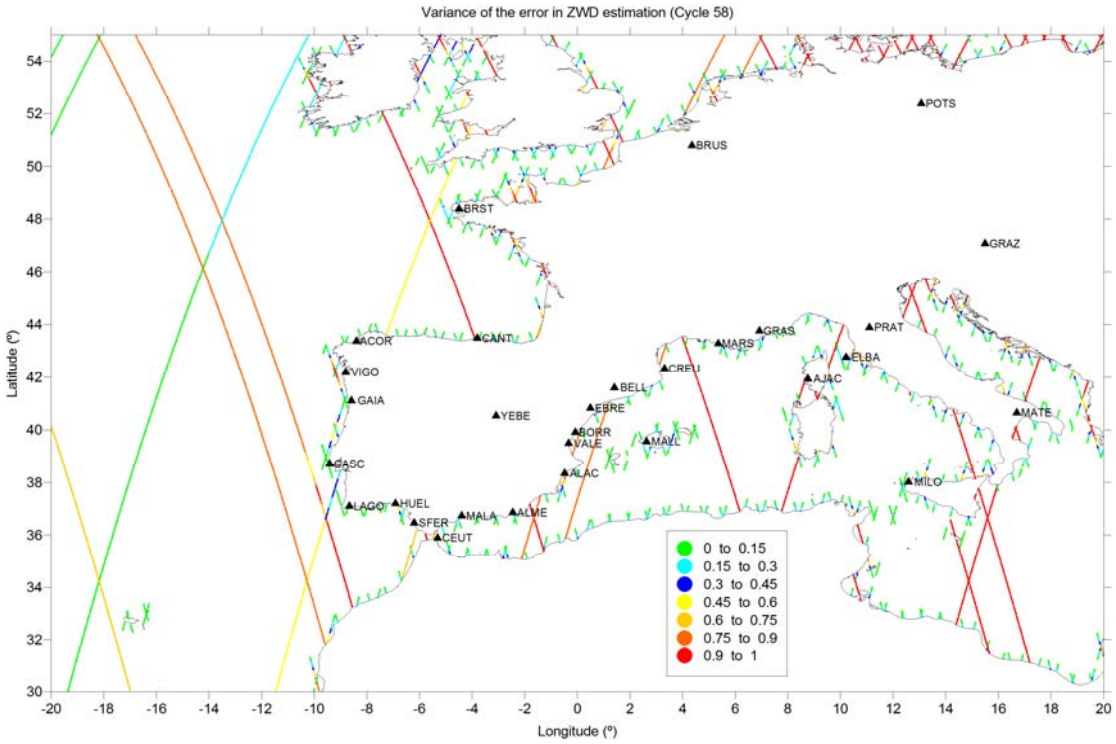

Fig.18 – Error variance associated with each ZWD-estimated value in percentage of the ZWD signal variance (assumed constant for the whole region and equal to 4 cm RMS). Black triangles show the location of the GNSS stations used in the data combination methodology.

ECMWF and microwave radiometer observations extracted from the GDR product (fields 41 and 42, respectively) are shown, in Figure 20, by the blue and red dots, in that order. There are two sets of consecutive flagged-as-invalid measurements, as can be verified by inspecting Figure 21: the first set occurs when the satellite approaches the southern coast of Portugal, close to LAGO station, and the second farther north, when the satellite approaches the coast close to CASC station.

The time intervals between the first and last invalid MWR measurements of these two sets are delimited by the grey and light blue shaded areas in Figure 20. Consecutive measurements with activated MWR land-ocean flag are delimited by the grey shaded areas (flag equal to 1) and consecutive measurements with MWR quality interpolation flag larger than 0 are delimited by the light blue shaded areas. The flag values are shown by the y-axis on the right side of the figure. In this particular case, the MWR quality interpolation flag is always set to 2, meaning that wet delay values were obtained by extrapolation (ESA 2006). In fact, it can be seen that wet delay estimates remain nearly constant in value in the light blue shaded areas (wet delay values are shown by the y-axis on the left side). The OA methodology has thus output wet delay estimates for all measurements represented by the red dots that are superimposed on the shaded areas, whichever its color, providing that these measurements have altimeter land-ocean flag equal to 0. The output values are shown in Figure 20 by the black dots.

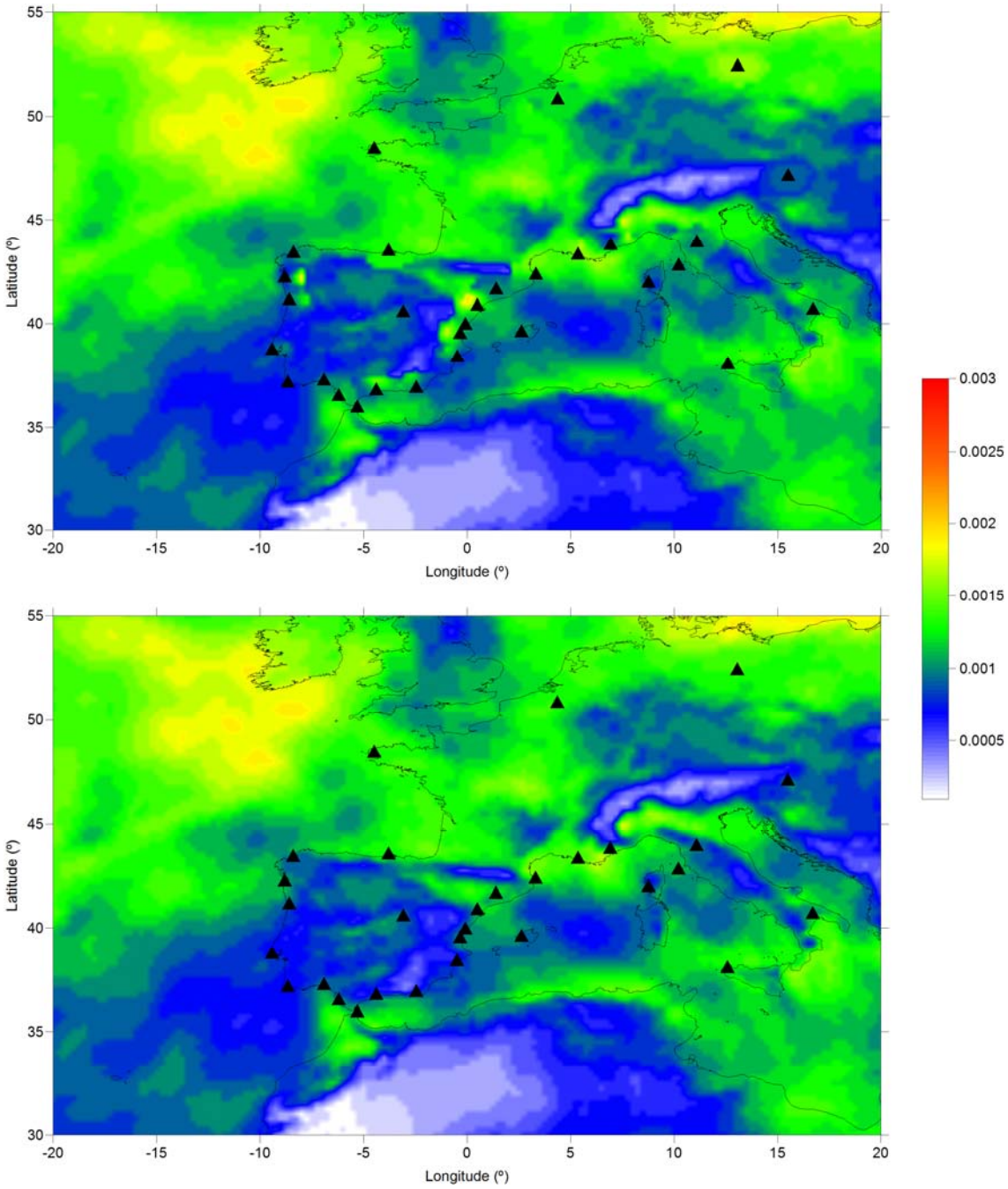

Fig.19 – ZWD variability calculated for the period corresponding to Envisat Cycle 58 (in m^2): (top) signal variability computed using the ZWD estimates output from the data combination methodology; (bottom) signal variability from ECMWF grids.

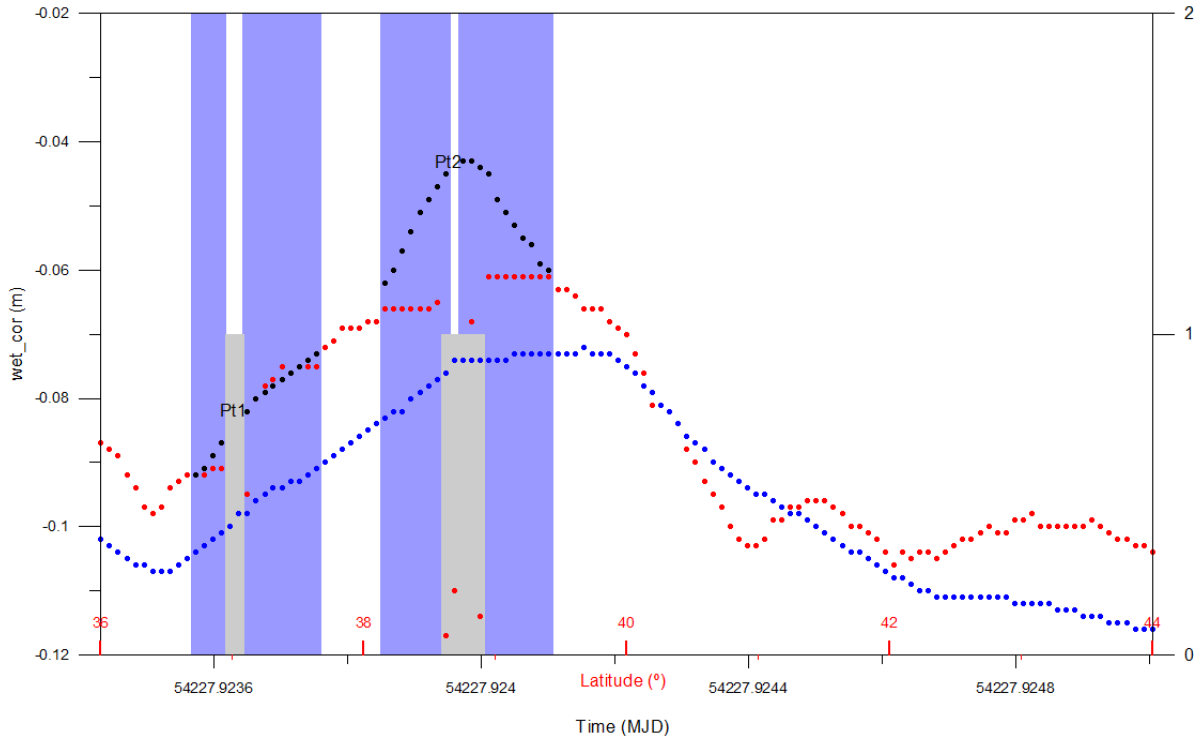

Fig.20 – Results obtained for Envisat pass 1 (Cycle 58) for the 36º-44ºN latitude range (see text for details). There are no GNSS-derived wet delay estimates acquired during the time interval shown on the x-axis.

Wet delay values for the first set of invalid measurements (shaded areas between 36º and 38ºN) seem to have been well estimated by the methodology. They show a tendency to increase with time analogous to that of the model ZWD values, and are clearly influenced by both the valid MWR and LAGO measurements. For instance, the ZWD value obtained for Point 1 (the one that lies immediately on the left of text Pt1 in the figure, with coordinates λ=-8.989186º, φ=37.14822º) was achieved considering 12 valid MWR measurements, 12 GNSS estimates from LAGO station and 41 values from one ECMWF-derived ZWD gridded map, in a total of 65 observations with mean value equal to -0.092 m. The distance between LAGO station and Pt1 is 29029.34 m, and its wet delay values have been acquired between approximately 0.111 days before and 0.118 days after the epoch that corresponds to Pt1 MWR measurement (being the minimum time interval equal to 0.007 days). Valid MWR measurements have been acquired almost simultaneously, but the closer measurement is at a distance of 52390.54 m from Pt1. Model observations are synoptic in time and referred to an epoch 0.076 days after that of Pt1 MWR acquisition. Only 5 points are at a distance smaller than that of the LAGO station (values between 11336.411 and 28433.979 m). The location of the observations used to compute the wet delay estimate for Pt1 is shown in Figure 21. The wet delay estimate of Pt1 has been updated to the value -0.088 m (GDR value is -0.095 m).

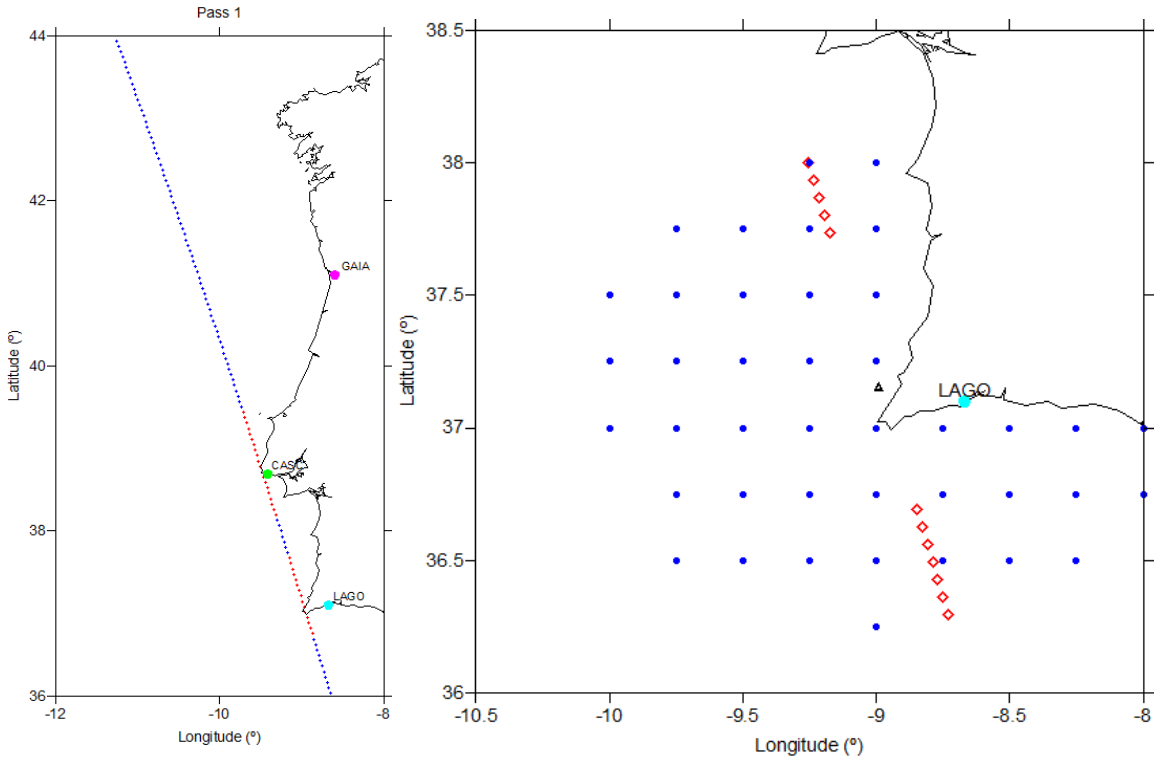

Fig.21 – (Left) Location of observations acquired during ENVISAT pass 1 (Cycle 58) in the 36º-44ºN latitudinal range (blue and red dots represent valid and invalid MWR wet delay values, respectively). (Right) Location of the observations used to update the wet delay estimate at the position represented by the black triangle (Pt1): model observations are represented by the blue dots, valid MWR measurements by the red lozenges and LAGO GNSS estimates by the cyan circle. Twelve observations from LAGO station have been used.

Wet delay values for the second set of invalid measurements (shaded areas comprised between latitudes 38º and 40ºN) are highly influenced by the GNSS-derived wet delay values of CASC station, especially at the locations where the selected valid MWR measurements are too far apart. The value obtained for Point 2 (immediately on the left of text Pt2 in the figure, with coordinates λ=-9.501673º, φ=38.784324º) was achieved considering 7 valid MWR measurements, 12 GNSS estimates from CASC station and 35 estimates from one ECMWF-derived ZWD gridded map (a total of 54 observations with a mean value of -0.068 m). The distance between CASC station and Pt2 is 12414.09 m, and its wet delay values have been acquired between approximately 0.111 days before and 0.118 days after the epoch that corresponds to Pt2 MWR measurement (the minimum time interval is 0.007 days). From the valid MWR measurements, the closest one is at a distance of 74838.379 m from Pt2. Time interval between model-derived observations and Pt2 is again 0.076 days and only 1 gridded point is at a distance smaller than that of the CASC station. The wet delay estimate for Pt2 has been updated from the GDR value of -0.074 m to the value -0.046 m (mean value of the 4 closest in time GNSS-derived measurements is -0.045 m). The values obtained by the methodology for the chosen latitudinal range were derived with a mapping error ranging from 1 to 9 percent of the signal variance. Situations like this one, therefore, need further analysis. In the absence of valid MWR measurements in the vicinity of the

locations where estimates are required, improved output values can only be achieved with a denser network of GNSS stations.

Figures 23, 24 and 25 show the results obtained for passes 74, 160 and 917 of Envisat Cycle 58, respectively. The y-axis on the right side of these figures now indicates the error associated with the wet delay estimates calculated by the data combination routine (in percentage of signal variance considered, at this stage, constant). The meaning of the shaded areas remains the same. The location of the microwave radiometer observations for these passes is shown in Figure 24. Red dots represent invalid MWR measurements, i.e., those for which the implemented methodology has updated the GDR wet delay values.

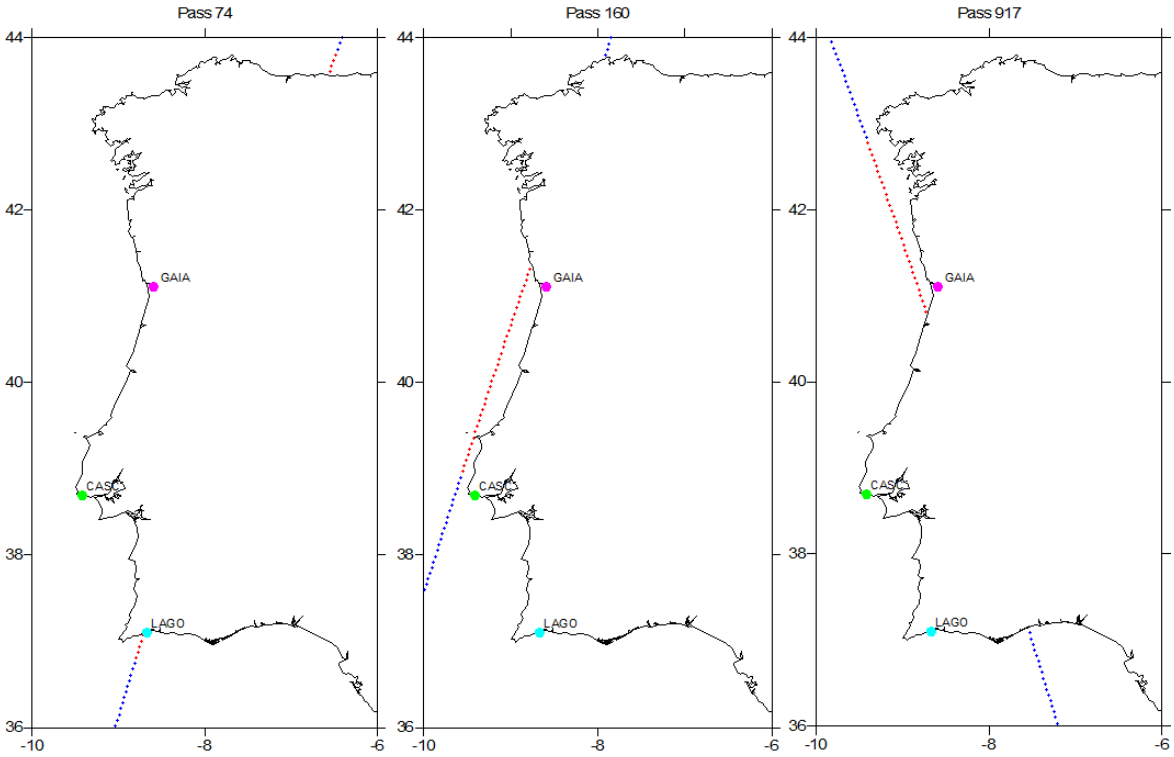

Fig.22 – Location of the microwave radiometer observations for Envisat passes 74, 160 and 917: blue dots represent valid MWR observations and red dots represent those flagged as invalid. The locations of the GNSS stations along the Portuguese coast (GAIA, CASC and LAGO) are also shown.

In general, the results show that when GNSS-derived wet delay values and valid MWR measurements are included in the selected observations, according to the chosen data selection criteria, the wet delay estimates that result from the application of the methodology are clearly influenced by them. Output values show clear departures from the ECMWF values present in the GDR product. However, in most of the cases, the variability of the field depicted by the ECMWF-derived values remains unchanged, i.e., when the ECMWF-derived values increase or decrease with time, the output field shows the same tendency. Based on the examples shown here, output values are thought to be better estimates of the field under analysis when compared to those derived from the ECMWF model and given in the GDR product.

Moreover, and in most of the analysed cases, there are no significant biases between the computed wet delay values and the immediately adjacent valid

MWR measurements. The continuity of the wet delay values is considered to be an added-value of the implemented methodology.

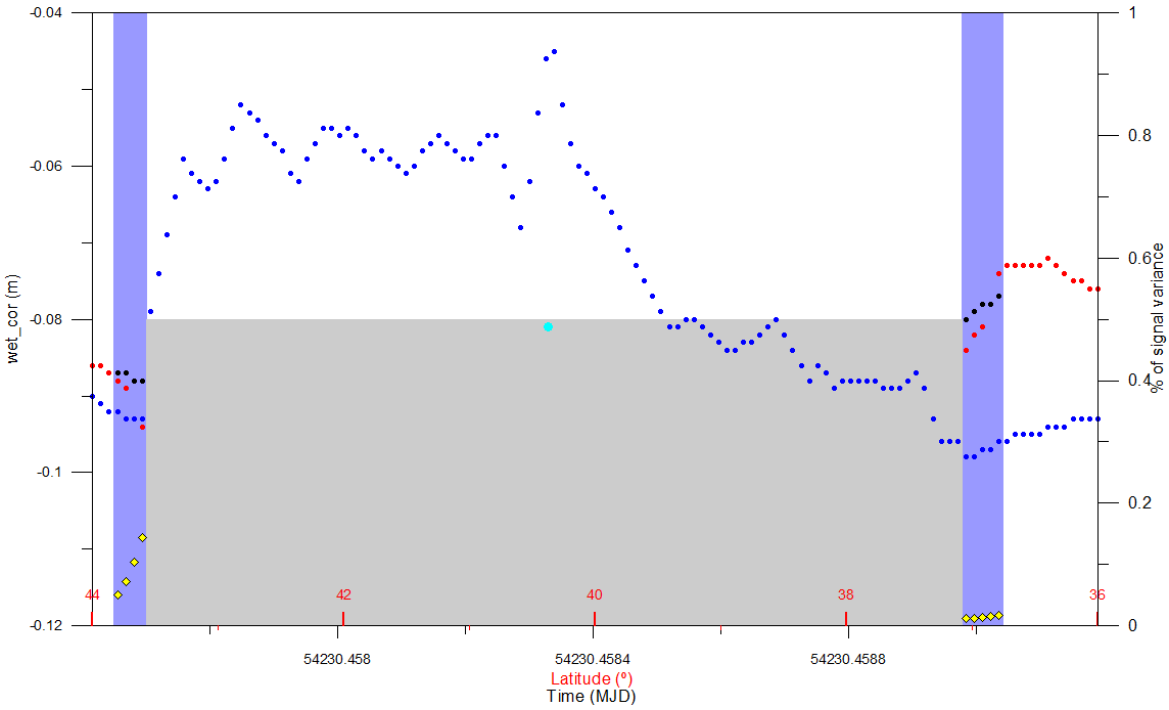

Fig.23 – Results obtained for Envisat pass 74 (Cycle 58) between 36° and 44°N. The cyan circle shows that a GNSS-derived wet delay value is comprised in the time interval shown in the x-axis. Yellow dots show the error in the estimations, given in percentage of the signal variance (referred to y-axis on the right). See text for details in the meaning of the shaded areas.

However, the implemented method is highly dependent on how good the estimate of the covariance function is. In the absence of in-depth information concerning the covariance function describing the spatial correlation between measurements, a simple positive-definite analytical function was chosen. In order to assure that the error variances are realistic, an analytical function must be fitted to the empirical covariance estimates. The fitting of the empirical auto-covariance function should also provide more accurate estimates of the correlation scales and, therefore, should give a new insight into the spatial and temporal variability of the field, supposed isotropic. Both the temporal and spatial correlation scales have been, at this stage, assumed to remain constant over the study region.

A constant variability of 4 cm RMS for the whole coastal study region has been chosen. The need for values of the signal variance for the locations where the MWR measurements are persistently contaminated is also stressed in order to achieve realistic relative mapping error values.

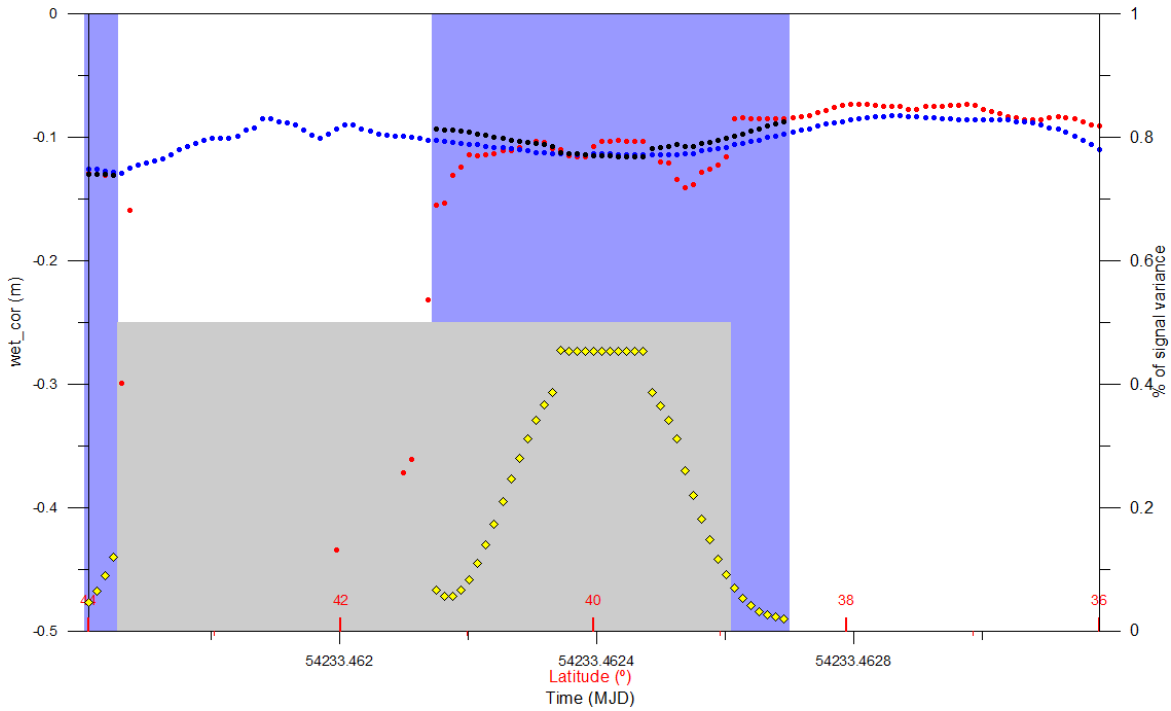

Fig.24 – Results obtained for Envisat pass 160 (Cycle 58) between 36° and 44°N (see text for details). There are no GNSS-derived wet delay estimates acquired during the time interval shown on the x-axis. Yellow dots show the error in the estimations, given in percentage of the signal variance (referred to y-axis on the right). See text for details in the meaning of the shaded areas.

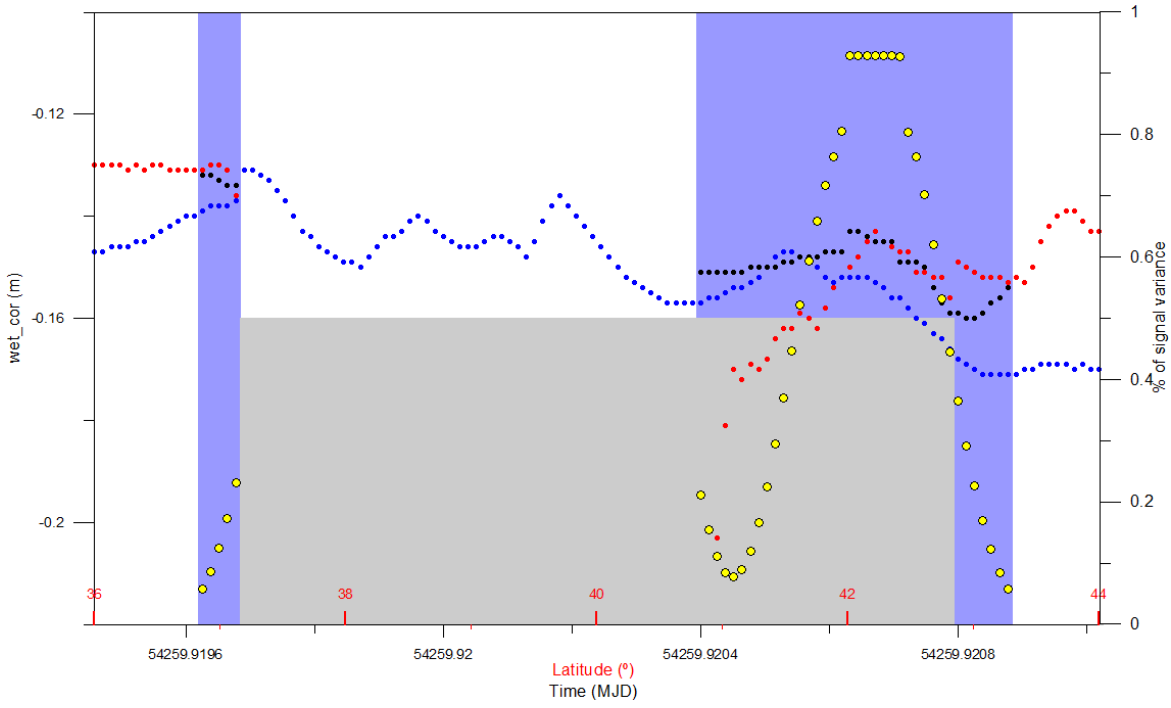

Fig.25 – Results obtained for Envisat pass 917 (Cycle 58) between 36° and 44°N (see text for details). There are no GNSS-derived wet delay estimates acquired during the time interval shown on the x-axis. Yellow dots show the error in the estimations, given in percentage of the signal variance (referred to y-axis on the right). See text for details in the meaning of the shaded areas.

4 Conclusions

The Dynamically-Linked Model (DLM) is a simple method that only requires GDR information, is mission-independent and can be used as a backup method whenever a more precise one is not available. This simple approach leads to a data recovery of more than 90% of the invalid measurements in the coastal regions, does not introduce discontinuities in the correction and can be used to generate coastal products in an operational processing scheme. Results show the DLM adjustment to ECMWF shall provide wet tropospheric corrections in the coastal region within an accuracy better than 1 cm.

The GNSS-derived Path Delay (GPD) is a very promising approach based on the combination of GNSS-derived path delays, valid microwave radiometer measurements and Numerical Weather Model (NWM) based information.

A comparison study between GNSS derived tropospheric delays and the corresponding fields present on altimeter products proved the suitability of the GNSS-derived tropospheric fields for use in the correction of the coastal altimeter measurements. Correlations between GNSS-derived tropospheric corrections and corresponding fields present on altimeter products are generally high, increasing with station proximity. Results show that the GNSS derived tropospheric delays seem to be appropriate to for use in the correction of the tropospheric delay for ocean locations up to one hundred kilometers away from the GNSS station.

Height reduction of GNSS-derived zenith delays to sea level is crucial. The methodology adopted, which applies separate reductions for ZHD and ZWD seems to be appropriate. UPorto GAMIT GNSS-derived ZHD+ZWD allow proper reduction of station height and separation between dry and wet components. Comparison with altimeter data reinforces the quality of the UPorto solutions for the tropospheric correction. EUREF solutions only provide Zenith Total Delay values at station level. Without ancillary meteorological data, it is not possible to perform the separation into ZHD and ZWD and therefore, to apply the required height reduction. However, present developments allow a proper separation of dry and wet components from the total path delay derived from GNSS measurements, even in the absence of *in situ* meteorological data.

At present, Uporto solutions provide zenith wet delays at sea level with an accuracy better than 1 cm.

It should be noted that as far as the tropospheric correction for coastal altimetry is concerned, providing GNSS-derived total correction seems to be as appropriate as providing the wet correction alone, since the dry component is independently derived with very high precision.

The data combination algorithm provides, for each invalid altimeter ground-track point, along with the wet tropospheric correction, the associated accuracy and an existing-output flag. Results show that when GNSS-derived wet delay values and valid MWR measurements are included in the selected observations, according to the established data selection criteria, the wet delay estimates that result from the application of the data combination methodology are clearly influenced by them. Output values show significant differences from the model wet correction present in the GDR product. However, in most cases, the variability of the field depicted by the model-derived values remains unchanged,

i.e., when they increase or decrease with time, the output field shows the same trend. Based on the results derived to date, output values are thought to be better estimates of the field under analysis when compared to the model-derived values given in the GDR product.

Moreover, no significant biases between the computed wet delay values and the immediately adjacent valid MWR measurements were found. The continuity of the wet delay values is considered to be an added-value of the implemented methodology.

Nevertheless, the accuracy of the final GPD product is expected to be highly dependent on data availability and distribution (GNSS stations and NWM) in both time and space.

Acknowledgements

The authors would like to acknowledge the European Centre for Medium Range Weather Forecasts (ECMWF) for providing the reanalysis data on the single-level atmospheric fields of the Deterministic Atmospheric Model and Dr. Pedro Viterbo from Instituto de Meteorologia for his personal commitment in facilitating the access to the referred data.

The authors would also like to acknowledge Radar Altimeter Database System (RADS) for providing the altimetric data and very gratefully thank Remko Scharroo (NOAA / Altimetrics LLC) for his prompt help and precious information about the data editing processes for the various altimeters.

References

Askne J, Nordius H (1987) Estimation of tropospheric delay for microwaves from surface weather data. Radio Science 22:379-386.

AVISO (2005) - Archiving, Validation and Interpretation of Satellite Oceanographic data, DT CorSSH and DT SLA Product Handbook, CLS-DOS-NT-05-097, Issue1 rev1, available at http://www.aviso.oceanobs.com/fileadmin/documents/data/tools/dt_corssh_dt_sla_products.pdf (May 2008).

Bai Z, Feng Y (2003) GPS water vapor estimation using interpolated surface meteorological data from Australian automatic weather stations. Journal of Global Positioning Systems 2(2):83-89

Bar-Sever YE, Kroger PM, Borjesson JA (1998) Estimating horizontal gradients of tropospheric path delay with a single GPS receiver. Journal of Geophysical Research 103(B3):5019-5035

Bevis M, Businger S, Herring TA, Rocken C, Anthes RA, Ware RH (1992) GPS Meteorology: Remote Sensing of Atmospheric Water Vapor Using the Global Positioning System. Journal of Geophysical Research 97(D14):15787-15801

Bevis M, Businger S, Chiswell S, Herring TA, ANthes, RA, Rocken C, Ware RH (1994) *GPS* Meteorology: Mapping Zenith Wet Delays onto Precipitable Water, Journal of Applied Meteorology, 33:379-386

Boehm J, Niell A, Tregoning P, Schuh H (2006) Global Mapping Functions (GMF): a new empirical mapping function based on numerical weather model data. Geophysical Research Letters 33(L07304) doi:10.1029/2005GL025546

Boehm J, Schuh H (2004) Vienna Mapping Functions in VLBI analyses. Geophysical Research Letters 31(L01603) doi:10.1029/2003GL018984

Bosser, P, Bock O, Pelon J, Thom C (2007) An Improved Mean-Gravity Model for GPS Hydrostatic Delay Calibration. IEEE Geoscience and Remote Sensing Letters 4(1):3-7

Bretherton, FP, Davis RE, Fandry CB (1976) A technique for objective analysis and design of oceanographic experiment applied to MODE-73. Deep-Sea Research 23:559-582

Chelton, DB, Ries JC, Haines BJ, Fu LL, Callahan PS (2001) Satellite Altimetry, In: Fu LL, Cazenave A (Eds.) Satellite Altimetry and Earth Sciences, International Geophysics Series, Vol. 69, Academic Press, pp. 1-131, ISBN: 0-12-269543-3

Dach R, Hugentobler U, Fridez P, Meindl M (Eds.) (2007) Bernese GPS Software - Version 5.0. Astronomical Institute, University of Bern

Davis JL, Herring TA, Shapiro II, Rogers AEE, Elgered G (1985) Geodesy by radio interferometry: effects of atmospheric modelling errors on estimates of baseline length. Radio Science 20(6):1593-1607

Desai SD, Haines BJ (2004) Monitoring Measurements from the Jason-1 Microwave Radiometer and Independent Validation with GPS. Marine Geodesy 27(1):221 – 240 doi:10.1080/01490410490465337

ECMWF (2009) http://www.ecmwf.int/products/catalogue/pseta.html

Edwards S, Moore P, King M (2004) Assessment of the Jason-1 and TOPEX/Poseidon Microwave Radiometer performance using GPS from offshore sites in the North Sea. Marine Geodesy, 27(3):717 – 727 doi:10.1080/01490410490883388

ESA (2006), ENVISAT RA-2 / MWR Level 2 User Manual V1.2, available in pdf at http://envisat.esa.int/pub/ESA_DOC/ENVISAT/RA2 MWR/PH_light_1rev2_ESA.pdf

Fernandes MJ, Bastos L, Antunes M (2003) Coastal Satellite Altimetry – Methods for Data Recovery and Validation, Proceedings of the 3rd Meeting of the International Gravity & Geoid Commission (GG2002), 302-307, Tziavos, IN (Ed.), Editions ZITI.

Hagemann S, Bengtsson L, Gendt G (2003) On the determination of atmospheric water vapor from GPS measurements. Journal of Geophysical Research 108(D21):4678 doi:10.1029/2002JD003235

Haines BJ, Bar-Sever YE (1998) Monitoring the TOPEX microwave radiometer with GPS: Stability of columnar water vapour measurements. Geophysical Research Letters 25(19):3563-3566

Herring T, King R, McClusky S (2006) GAMIT Reference Manual – GPS Analysis at MIT - Release 10.3. Department of Earth, Atmospheric and Planetary Sciences, Massachusetts Institute of Technology

Hopfield HS (1971) Tropospheric effect on electromagnetic measured range: prediction from surface weather data. Radio Science 6:357-367

Kouba J (2008) Implementation and testing of the gridded Vienna Mapping Function 1 (VMF1). Journal of Geodesy 82:193-205 doi:10.1007/s00190-007-0170-0

Marini JW (1972) Correction of satellite tracking data for an arbitrary tropospheric profile. Radio Science 7(2):223– 231

Mendes VB, Prates G, Santos L, Langley RB (2000) An Evaluation of the Accuracy of Models of the Determination of the Weighted Mean Temperature of the Atmosphere. Proceedings of ION, 2000 National Technical Meeting, January 26-28, 2000, Pacific Hotel Disneyland, Anaheim, CA

Mercier F (2004) Amélioration de la correction de troposphère humide en zone côtière. Rapport Gocina, CLS-DOS-NT-04-086

Moore P, Edwards E, King M (2005) Radiometric path delay calibration of ERS-2 with application to altimetric range. Proceedings of the 2004 Envisat & ERS Symposium, Salzburg, Austria 6-10 September 2004

Niell AE (1996) Global mapping functions for the atmosphere delay at radio wavelengths. Journal of Geophysical Research 101(B2):3277-3246

Niell AE (2001) Preliminary evaluation of atmospheric mapping functions based on numerical weather models. Physics and Chemistry of the Earth 26:475–480

Niell AE, Coster AJ, Solheim FS, Mendes VB, Toor PC, Langley RB, Upham CA (2001) Comparison of Measurements of Atmospheric Wet Delay by Radiosonde, Water Vapor Radiometer, GPS, and VLBI. Journal of Atmospheric and Oceanic Technology 18:830-850

Saastamoinen J (1972) Atmospheric correction for troposphere and stratosphere in radio ranging of satellites. In Henriksen S, Mancini A, Chovitz B (Eds.) The use of artificial satellites for geodesy, 15:247-251, Geophysics Monograph Series, AGU, Washington D.C.

Scharroo R, Lillibridge JL, Smith WHF, Schrama, EJO Cross-calibration and long-term monitoring of the microwave radiometers of ERS, TOPEX, GFO, Jason and Envisat. Marine Geodesy 27:279–297 (2004).

Schüler T (2001) On Ground-Based GPS Tropospheric Delay Estimation. PhD Thesis, Universität der Bundeswehr München, Studiengang Geodäsie und Geoinformation available at http://ub.unibw-muenchen.de/dissertationen/ediss/schueler-torben/inhalt.pdf Accessed 13 January 2009

Smith EK, Weintraub S (1953) The constants in the equation for atmospheric refractive index at radio frequencies. Proceedings of the Institute of Radio Engineers 41(8):1035-1037

Snajdrova K, Boehm J, Willis P, Haas R, Schuh H (2006) Multi-technique comparison of tropospheric zenith delays derived during the CONT02 campaign. Journal of Geodesy 79:613–623 doi: 10.1007/s00190-005-0010-z

Wang J, Zhang L, Dai A, Van Hove T, Van Baelen J (2007) A near-global, 2-hourly data set of atmospheric precipitable water from ground-based GPS

measurements. Journal of Geophysical Research 112(D11107)doi:10.1029/2006JD007529;

Webb FH, Zumberge JF (1995) An introduction to GIPSY/OASIS-II. JPL Publication D-11088, Jet Propulsion Laboratory, Pasadena